

Exact wavefield extrapolation in 2D for $v(x)$

Gary F. Margrave, Michael P. Lamoureux, Peter Gibson, Richard A. Bale,
and Jeff Grossman

ABSTRACT

We pose the wavefield extrapolation problem in two spatial dimensions for arbitrary lateral velocity variation, $v(x)$. Then, by restricting attention to the discretely sampled case, we develop an exact solution via an eigenvalue decomposition. The matrix that is decomposed is the difference between a diagonal matrix containing the squared horizontal wavenumbers and a Toeplitz matrix, scaled by frequency squared, containing the Fourier transform of the square on the inverse velocity. This solution gives an explicit decomposition of a wavefield into independent upward and downward travelling parts.

We also analyze the continuous problem via functional analytic methods and, though we fail to reach a general solution, we demonstrate the independence of upward- and downward-travelling waves. In the specific case of the step velocity function, we calculate the eigenfunctions and exhibit a formula that determines the eigenvalues, though the latter must be solved numerically.

Numerical testing shows that the exact extrapolator produces physically understandable result. When compared with three different approximate extrapolators based on Fourier integral operators, the approximate operators can be grossly wrong if a large extrapolation step is taken in the presence of strong velocity gradients. However, if the approximate operators are used in a recursion taking many small steps, they appear to approach the correct result. In a simulation of inversion with an erroneous velocity model, the three approximate extrapolators produce a very similar result to the exact extrapolator. This indicates that a very precise velocity model is required to take advantage of the exact extrapolator.

INTRODUCTION

Wavefield extrapolation is the central technology in the class of migration algorithms that, in somewhat inappropriate¹ popular jargon, are commonly called *wave equation* methods. Usually applied in a marching scheme over depth, these methods are more appropriately called *recursive wavefield extrapolation* methods. Perhaps the first examples of such methods were the finite-difference techniques developed by Jon Claerbout and colleagues (see Claerbout, 1976). Later, other methods were developed such as *phase shift* (Gazdag, 1978), *space-frequency extrapolation* (Berkhout, 1981), *phase shift plus interpolation* (Gazdag and Squazzerro, 1984), *split-step Fourier* (Stoffa et al., 1989), *phase-screen* (Wu, 1992, 1994), *generalized screen methods* (Le Rousseau and de Hoop, 2001), *nonstationary phase shift* (Margrave and Ferguson, 1999, Ferguson and Margrave, 2002) and *recursive Kirchhoff* (Bevc, 1997, Margrave and Daley, 2001, Margrave and Geiger, 2002) were developed.

¹ Inappropriate because all successful migration algorithms have a wave equation as their basis.

For variable velocity, all of these extrapolation methods are approximate, and it is useful to have an exact solution to compare them to. Grimbergen et al. (1998) presented a nearly exact solution based on an eigenvalue decomposition in the (x, ω) domain for the discrete, 2D, problem. Their method handled arbitrary lateral velocity variations and arbitrary scattering angles (i.e. dips) but was approximate in that $\partial^2/\partial x^2$ was represented by a standard three-point central difference operator. Yao and Margrave (1999 and 2000) presented the method discussed here which is exact in the 2D discrete case, though its use of discrete Fourier transforms means that wraparound is a significant problem. Yao and Margrave also use an eigenvalue decomposition but in the (k_x, ω) domain where the $\partial^2/\partial x^2$ term can be accomplished exactly. Here we re-examine the Fourier-eigenvalue method of Yao and Margrave because: (1) the original solution technique was unnecessarily complex; (2) it is not well-known that this exact solution exists; (3) we wish to compare it with the approximate nonstationary phase shift methods; and (4) we are interested in its possible generalizations.

In the next section we present a simplified and rigorous derivation of the exact Fourier-eigenvalue solution. We begin by posing the problem in the continuous case and reducing it to an integro-differential equation in the (k_x, ω) domain. We then pass to the discrete (i.e. discretely-sampled) case and reduce the integral equation to a matrix equation that can be subjected to eigenvalue decomposition. The matrix involved consists of a diagonal matrix, with the values of k_x^2 down the diagonal, minus ω^2 times a Toeplitz matrix whose entries are the Fourier transform of $v^{-2}(x)$. This eigenvalue decomposition appears to always be possible (we have no proof of this) though it gets very expensive for large matrices. Given an eigenvalue decomposition, we present the general, exact solution to the wavefield extrapolation problem assuming the presence of both upward-travelling and downward-travelling waves. For the common seismic problem, we also give the solution for only upward-travelling waves. In a subsequent numerical example, we demonstrate that our exact solution is highly impacted by Fourier wraparound and, to control this, we introduce numerical dissipation through the artifice of a complex velocity. In our numerical examples, we explore the relationship between the exact solution and the approximate nonstationary phase-shift extrapolators. In particular, we show that the latter converge upon the exact result when applied in a recursion using very small depth steps.

DERIVATION OF THE EXACT 2D EXTRAPOLATOR

Posing the problem in the continuous case

Let $\Psi(x, z, t)$ be a 2D scalar wavefield that obeys the wave equation,

$$\frac{\partial^2}{\partial x^2} \Psi(x, z, t) + \frac{\partial^2}{\partial z^2} \Psi(x, z, t) = \frac{1}{v^2(x)} \frac{\partial^2}{\partial t^2} \Psi(x, z, t), \quad (1)$$

where we note that the velocity, $v(x)$, is assumed to be independent of the vertical coordinate, z , but has arbitrary dependence upon the lateral coordinate, x . Letting $\psi(x, z, \omega)$ be the Fourier transform over time of $\Psi(x, z, t)$ as given by

$$\psi(x, z, \omega) = \int_{\mathbb{R}} \Psi(x, z, t) e^{-i\omega t} dt, \quad (2)$$

where the subscript \mathbb{R} indicates that the integration is over the entire real line, then equation (1) leads to the Helmholtz equation for $\psi(x, z, \omega)$,

$$\frac{\partial^2}{\partial x^2} \psi(x, z, \omega) + \frac{\partial^2}{\partial z^2} \psi(x, z, \omega) = \frac{-\omega^2}{v^2(x)} \psi(x, z, \omega). \quad (3)$$

Now, we employ a further Fourier transform over the lateral coordinate, x , and obtain

$$k_x^2 \hat{\psi}(k_x, z, \omega) + \frac{\partial^2}{\partial z^2} \hat{\psi}(k_x, z, \omega) = -\omega^2 \hat{s} \bullet \hat{\psi}(k_x, z, \omega) \quad (4)$$

where the hat, $\hat{\cdot}$, denotes the spatial Fourier transform as in

$$\hat{\psi}(k_x, z, \omega) = \int_{\mathbb{R}} \psi(x, z, \omega) e^{ik_x x} dx, \quad (5)$$

the bullet (\bullet) denotes convolution over lateral wavenumber, k_x , and we have defined

$$s(x) = v^{-2}(x). \quad (6)$$

The use of different signs in the complex exponential functions of equations (2) and (5) is deliberate. We rearrange equation (4) to write

$$\frac{\partial^2}{\partial z^2} \hat{\psi}(k_x, z, \omega) = \int_{\mathbb{R}} \left[m^2 \delta(k_x - m) - \omega^2 \hat{s}(k_x - m) \right] \hat{\psi}(m, z, \omega) dm, \quad (7)$$

or

$$\frac{\partial^2}{\partial z^2} \hat{\psi}(k_x, z, \omega) = - \int_{\mathbb{R}} M(m, k_x, \omega) \hat{\psi}(m, z, \omega) dm, \quad (8)$$

where

$$M(m, k_x, \omega) = -m^2 \delta(k_x - m) + \omega^2 \hat{s}(k_x - m). \quad (9)$$

Solution of the discretely sampled case

We now assume that $\psi(x, z, \omega)$ and $\hat{\psi}(k_x, z, \omega)$ are regularly sampled in x and k_x respectively. Furthermore, we represent these wavefields as column vectors (of k_x variation with constant ω) and the integration of equation (8) as a matrix-vector product,

$$\frac{\partial^2}{\partial z^2} \begin{bmatrix} \hat{\psi}_0 \\ \hat{\psi}_1 \\ \vdots \\ \hat{\psi}_n \end{bmatrix} = \begin{bmatrix} M_{0,0} & M_{0,1} & \cdots & M_{0,n} \\ M_{1,0} & M_{1,1} & & \\ \vdots & & \ddots & \\ M_{n,0} & & & M_{n,n} \end{bmatrix} \begin{bmatrix} \hat{\psi}_0 \\ \hat{\psi}_1 \\ \vdots \\ \hat{\psi}_n \end{bmatrix}, \quad (10)$$

or symbolically,

$$\frac{\partial^2}{\partial z^2} \underline{\hat{\psi}} = -\underline{\underline{M}} \underline{\hat{\psi}}. \quad (11)$$

The matrix, $\underline{\underline{M}}$, is the difference between a diagonal matrix containing the squares of the horizontal wavenumber and a Toeplitz matrix representing convolution with $\omega^2 \hat{s}$

$$\underline{\underline{M}} = - \begin{bmatrix} k_{x0}^2 & & & 0 \\ & k_{x1}^2 & & \\ & & \ddots & \\ 0 & & & k_{xn}^2 \end{bmatrix} + \omega^2 \begin{bmatrix} \hat{s}_0 & \hat{s}_{-1} & \cdots & \hat{s}_{-n} \\ \hat{s}_1 & \hat{s}_0 & \hat{s}_{-1} & \\ \vdots & \hat{s}_1 & \ddots & \\ \hat{s}_n & & & \hat{s}_0 \end{bmatrix}. \quad (12)$$

Matrix $\underline{\underline{M}}$ can be written as an eigenvalue decomposition as

$$\underline{\underline{M}} = \underline{\underline{U}} \underline{\underline{\Lambda}} \underline{\underline{U}}^{-1} \quad (13)$$

where $\underline{\underline{U}}$ is the eigenvector matrix and $\underline{\underline{\Lambda}}$ a diagonal matrix with the eigenvalues of $\underline{\underline{M}}$ on the diagonal. According to Strang (1986), almost every square matrix can be decomposed in this way though certain matrices have simpler decompositions. For example, a self-adjoint matrix (i.e., a matrix that is equal to the complex conjugate of its transpose) has real eigenvalues and orthogonal eigenvectors. This means that the inverse of the eigenvector matrix, $\underline{\underline{U}}$ is just its adjoint $\underline{\underline{U}}^{-1} = \underline{\underline{U}}^\dagger$. The matrix $\underline{\underline{M}}$ in equation 12 is easily shown to be a linear combination of two self-adjoint matrices and is therefore self-adjoint. However, in the next section we will introduce a small imaginary component of velocity to control Fourier wrap-around via a numerical attenuation. This destroys the self-adjoint property so we retain the notation $\underline{\underline{U}}^{-1}$.

Now defining

$$\underline{\tilde{\psi}} = \underline{U}^{-1} \hat{\underline{\psi}} \quad (14)$$

equation (11) transforms to

$$\frac{\partial^2}{\partial z^2} \underline{\tilde{\psi}} = -\underline{\Lambda} \underline{\tilde{\psi}}. \quad (15)$$

Let $\underline{\lambda}$ denote the diagonal entries of $\underline{\Lambda}$ (the eigenvalues) and then equation (15) has the general solution

$$\underline{\tilde{\psi}} = A e^{i\sqrt[+]{\underline{\lambda}}z} + B e^{-i\sqrt[+]{\underline{\lambda}}z} \quad (16)$$

where by $\sqrt[+]{\underline{\lambda}}$ we mean the positive square root of each element of $\underline{\lambda}$ and A and B are constants to be determined from the boundary conditions. The solution for $\Psi(x, z, t)$ is then

$$\Psi(x, z, t) = \int e^{i\omega t} \left[F_{k_x \rightarrow x}^{-1} \left(U \left\{ A e^{i\sqrt[+]{\underline{\lambda}}z} + B e^{-i\sqrt[+]{\underline{\lambda}}z} \right\} \right) \right] d\omega, \quad (17)$$

where $F_{k_x \rightarrow x}^{-1}$ is the inverse discrete Fourier transform from k_x to x . From this result, and assuming that the z coordinate is increasing downwards, it is apparent that $A e^{i\sqrt[+]{\underline{\lambda}}z}$ represents *upward-travelling waves* while $B e^{-i\sqrt[+]{\underline{\lambda}}z}$ has the interpretation of *downward-travelling waves*.

Thus we have an explicit, exact solution to the 2D, discrete wavefield extrapolation problem. Fishman and McCoy (1985) showed that it is always possible to *factorize* the Helmholtz equation, when velocity is a function only of the transverse coordinates, into terms representing upward- and downward-travelling waves. That is, upward- and downward-travelling waves are coupled (not independent) only if $\partial v / \partial z \neq 0$. Fishman and McCoy exhibited only approximate forms for the wavefield factors. Equation (17) is an exact realization of the factorization in the specific 2D, discrete case.

Boundary conditions and the explicit solution

For a general solution, Cauchy boundary conditions are required on an open surface for hyperbolic PDE's such as the scalar wave equation. That is, given the values of $\Psi(x, z=0, t)$ and $\partial_z \Psi(x, z, t)|_{z=0}$ (the vertical gradient of the wavefield) on the surface $z=0$, we can develop two equations that determine the unknown constants A and B , namely

$$\begin{aligned}\tilde{\psi}(k_x, z=0, \omega) &= A + B \\ \frac{\partial}{\partial z} \tilde{\psi}(k_x, z, \omega) \Big|_{z=0} &= i\sqrt[3]{\underline{\lambda}}A - i\sqrt[3]{\underline{\lambda}}B\end{aligned}\quad (18)$$

from which A and B can be uniquely determined. In this expression,

$$\tilde{\psi}(k_x, z=0, \omega) = \underline{\underline{U}}^{-1} \left(F_{x \rightarrow k_x} \left[\int_{\mathbb{R}} \Psi(x, z=0, t) e^{-i\omega t} dt \right] \right) \quad (19)$$

is the suitably transformed boundary wavefield and similarly for the boundary gradient.

When inserted into equation (17) we have an expression for the exact extrapolation of the total wavefield from $z=0$ to any other datum (i.e. surface of $z = \text{constant}$). However, in the seismic imaging problem, $\partial_z \Psi(x, z, t) \Big|_{z=0}$ is not readily available; consequently, we make the common assumption that $\Psi(x, z, t)$ contains only upward-travelling waves and so develop the general extrapolation equation,

$$\Psi(x, z, t) = \int e^{i\omega t} \left[F_{k_x \rightarrow x}^{-1} \left(\underline{\underline{U}} \left\{ \tilde{\psi}(k_x, z=0, \omega) e^{i\sqrt[3]{\underline{\lambda}}z} \right\} \right) \right] d\omega. \quad (20)$$

Equation (20) provides the complete, exact extrapolator in the (x, z, t) domain. In the eigenvalue domain, there is a much simpler extrapolation expression

$$\tilde{\psi}(z) = \tilde{\psi}(z=0) e^{i\sqrt[3]{\underline{\lambda}}z}. \quad (21)$$

In using equation (21) or equation (20) care must be taken to properly handle the case when $\underline{\lambda} < 0$ as this generates real-valued exponential decay or growth instead of the wavelike oscillations when $\underline{\lambda} > 0$. We reject the possibility of exponentially growing solutions on physical grounds and modify equation (21) to read

$$\tilde{\psi}(z) = \tilde{\psi}(z=0) e^{iz \operatorname{real}(\sqrt[3]{\underline{\lambda}}) - |z \operatorname{imag}(\sqrt[3]{\underline{\lambda}})|}. \quad (22)$$

Equation (20) can be similarly modified.

Investigation of the continuous case

While we have not solved the continuous case, we have been able to draw some interesting conclusions. Returning to the Helmholtz equation (equation 3), we rearrange it as

$$\frac{\partial^2}{\partial z^2} \psi(x, z, \omega) = -\frac{\partial^2}{\partial x^2} \psi(x, z, \omega) - \frac{\omega^2}{v^2(x)} \psi(x, z, \omega) \quad (23a)$$

and convert to a parameterized functional equation

$$\frac{d^2}{dz^2}u = -A_\omega u \quad (23b)$$

where we treat u as a map from the real line \mathbb{R} to the space $L^2(\mathbb{R})$ of square integrable functions, and A_ω a (parameterized) differential operator on $L^2(\mathbb{R})$. More precisely, each function $u(z) \in L^2(\mathbb{R})$ evaluates pointwise as

$$u(z)(x) = \psi(x, z, \omega) \quad (24)$$

and A_ω is a map, from a dense subset of differentiable functions ϕ in $L^2(\mathbb{R})$ into $L^2(\mathbb{R})$, given as

$$(A_\omega \phi)(x) = \phi''(x) + \frac{\omega^2}{v^2(x)} \phi(x). \quad (25)$$

For real parameter ω and velocity field $v(x)$, and reasonable boundary conditions defining the domain of operator A_ω , this operator is an unbounded self-adjoint operator on $L^2(\mathbb{R})$. Thus the functional calculus may be applied and we can compute directly with the operator A_ω . In particular, the square root $A_\omega^{1/2}$ exists, and the solution to the functional equation is given by the usual exponential form for an ordinary differential equation with operator A_ω playing the role of a “constant”. Then, the function u in the form

$$u(z) = e^{izA_\omega^{1/2}} \phi_1 + e^{-izA_\omega^{1/2}} \phi_2 \quad (26)$$

is the general solution to the functional form of the Helmholtz equation.

Cauchy boundary conditions determine functions ϕ_1 and ϕ_2 uniquely, via the 2 by 2 linear system,

$$u(0) = \phi_1 + \phi_2 \quad (27)$$

$$u'(0) = iA_\omega^{1/2}(\phi_1 - \phi_2). \quad (28)$$

However, in a typical seismic experiment, it is common to interpret the two exponentials as representing the sum of upward-travelling waves with downward-travelling waves, and eliminate one of the two as appropriate for the physics of the experiment. Which term is upward, and which is downward, depends on the particular choice of the square root operator.

Computing the operators $e^{izA_\omega^{1/2}}$ and $e^{-izA_\omega^{1/2}}$ involves performing an infinite dimensional eigenvalue decomposition for the self-adjoint operator A_ω . Formally, one may write

$$e^{izA_\omega^{1/2}} = \int_{-\infty}^{\infty} e^{iz\lambda^{1/2}} dP_\lambda \quad (29)$$

where $\{P_\lambda\}$ is a projection-valued measure on $L^2(\mathbb{R})$ coming from the spectral decomposition of the operator A_ω . Actually computing this operator for a general velocity field $v(x)$ is quite complex and not practical for real geophysical problems. So, instead of finding a general solution, we will consider an exact solution for an artificial, but basic case of interest, useful for testing other approximate solutions.

We consider a stepped velocity wavefield

$$v(x) = \begin{cases} v_- & x < 0 \\ v_+ & x > 0. \end{cases} \quad (30)$$

To compute the spectral decomposition for A_ω , we find the eigenfunction solutions to

$$A_\omega \psi_k = k^2 \psi_k, \quad (31)$$

where k^2 denotes the corresponding eigenvalue, and for which k will be the eigenvalue for $A_\omega^{1/2}$. Since A_ω is self-adjoint, the eigenvalue k^2 is necessarily real, but possibly negative. Thus we allow for the possibility that k may be real or imaginary.

The eigen-equation is a second-order, ordinary differential equation in x , with constant coefficients on each of the two halves of the real line, so the solution is easily obtained in the form

$$\psi_k(x) = \begin{cases} ae^{ix\sqrt{k^2-\omega^2/v_-^2}} + be^{-ix\sqrt{k^2-\omega^2/v_-^2}} & x < 0 \\ ce^{ix\sqrt{k^2-\omega^2/v_+^2}} + de^{-ix\sqrt{k^2-\omega^2/v_+^2}} & x > 0 \end{cases} \quad (32)$$

The scalars a, b, c, d are chosen so that the function ψ_k and its first derivative are continuous across $x=0$ and satisfy the given boundary conditions. When A_ω has no boundary (i.e. $-\infty < x < \infty$), there is a continuum, of eigenvalues, a situation we don't wish to explore here. With finite boundary ($-L \leq x \leq L$), the spectrum of A_ω is an unbounded sequence of discrete points on the real line.

At least two standard choices are available for a self-adjoint, finite boundary condition: the usual Dirichlet condition

$$\psi_k(\pm L) = 0 \quad (33)$$

and the Neumann condition

$$\phi'_k(\pm L) = 0. \quad (34)$$

Either condition will force reflections at the artificial boundaries $x = \pm L$, which is a non-physical artefact of the mathematical model for the seismic imaging experiment. However, by taking L sufficiently large, we may assume this boundary is sufficiently far away for the seismic sources and receivers to cause no interference (in a given finite amount of time). For definiteness, let us take Dirichlet boundary conditions.

For the Dirichlet boundary condition, the condition that ψ_k vanish at the endpoints simplifies the solution to the form

$$\psi_k(x) = \begin{cases} a' \sin(\kappa_-(x+L)) & x < 0 \\ b' \sin(\kappa_+(x-L)) & x > 0 \end{cases} \quad (35)$$

where we have introduced the quantities $\kappa_- = \sqrt{k^2 - \omega^2 / v_-^2}$ and $\kappa_+ = \sqrt{k^2 - \omega^2 / v_+^2}$. Continuity for the function and its derivative across the point $x = 0$ requires

$$a' \sin(\kappa_- L) = -b' \sin(\kappa_+ L) \quad (36)$$

and

$$a' \kappa_- \cos(\kappa_- L) = b' \kappa_+ \cos(\kappa_+ L), \quad (37)$$

from which we conclude that

$$\frac{\tan(\kappa_+ L)}{\kappa_+} = -\frac{\tan(\kappa_- L)}{\kappa_-}. \quad (38)$$

Remembering that κ_+ and κ_- are related through the parameter k^2 , this last equation implies that only a discrete set of value for k^2 allows for a solution. Thus the spectrum is discrete.

In the trivial case of $v_+ = v_-$ (constant velocity field), the only solutions are when κL is a multiple of π , and thus $k^2 = \omega^2 / v^2 + n^2 \pi^2 / L^2$, for some integer n , as expected. When the velocities v_+, v_- are different, equation (38) can be solved numerically; however, we are unaware of an analytical formula that finds this set of values for k^2 .

When κ_+ and κ_- are both positive, the eigenfunction is simply two sine waves of different frequencies joined together smoothly at $x = 0$. If one of the κ is imaginary, we have a sine wave joined to a hyperbolic sine (a sum of exponentials). This situation gives

evanescent waves for the imaginary κ , which are an important component of a complete wavefield simulation. If both of the κ 's are imaginary, no solution is possible.

Once these eigenvalues are found as discrete solutions to equation (38), the rest of the analysis is routine. The eigenfunctions ϕ_k are normalized so their $L^2[-L, L]$ norm is one; any function ϕ in the space can be expanded as a superposition of these eigenfunctions

$$\phi = \sum_k \langle \phi, \phi_k \rangle \phi_k ; \quad (39)$$

and the action of the operators A_ω , $A_\omega^{1/2}$, and $e^{izA_\omega^{1/2}}$ are given via their action on eigenfunctions. For instance

$$A_\omega^{1/2} \phi = \sum_k k \langle \phi, \phi_k \rangle \phi_k \quad (40)$$

and

$$e^{izA_\omega^{1/2}} \phi = \sum_k e^{izk} \langle \phi, \phi_k \rangle \phi_k . \quad (41)$$

Unfortunately, since the discrete eigenvalues are not uniformly spaced, a Fast Fourier Transform (FFT) is not available to compute the coefficients $\langle \phi, \phi_k \rangle$.

While we were not able to construct a solution for general $v(x)$, we were able to demonstrate the Fishman and McCoy (1985) conclusion that upward- and downward-travelling waves are completely independent. Also, we were able to obtain a nearly analytical formula for the prototypical stepped velocity case on a finite interval. Our formula requires a numerical calculation of the eigenvalues from a transcendental expression arising from the boundary conditions.

A 2D NUMERICAL IMPLEMENTATION

Here we present a simple numerical implementation in the MATLAB language. Early in its implementation, a major problem related to Fourier wraparound was encountered. Figure 1 shows a simple step velocity model superimposed on an assumed input wavefield ($\Psi(x, z=0, t)$) containing a single bandlimited impulse positioned just to the left of the velocity step. In Figure 2, the result of a direct implementation of the exact algorithm is shown for an extrapolation step of 200 metres upward. This result is highly unsatisfactory because it is dominated by unwanted algorithmic artefacts. To demonstrate this, Figure 3 is another extrapolation, identical in all respects except that the velocity function was given a small (1%) imaginary component. This causes all elements of $\sqrt{\lambda}$ to have small imaginary components and, in the light of equation (22) will cause a small, artificial attenuation that is much like a Q effect. Thus events with larger traveltimes suffer greater attenuation and Fourier wraparound is effectively reduced. There are three obvious events remaining in Figure 3, all with direct physical explanations. Thus we conjecture that the events and noise in Figure 2 that are not obviously present in Figure 3

result from the superposition of Fourier wrap-around effects. Since there are infinitely many periodic ‘aliases’ of the desired model induced in \mathbb{R}^2 by the two-dimensional DFT (over (x, t)), the wraparound can be very strong. All remaining results shown in this paper use this 1% imaginary velocity adjustment.

The exact algorithm presented in this paper is computationally intensive and is probably not viable in a seismic imaging method at present. However, it is still very useful because it can be compared with various faster, though approximate techniques. Here we examine the NSPS (*nonstationary phase shift*) and generalized PSPI (*phase shift plus interpolation*) methods presented in Margrave and Ferguson (1999). Also, we look at the Weyl extrapolator presented in Margrave and Ferguson (1998) and Margrave and Daley (2001). In assessing the results to come, it must be remembered that the PSPI results shown here are not computed through any sort of interpolation scheme between reference velocities. Rather, the generalized PSPI (GPSPI hereafter) algorithm is formulated as a Fourier integral operator that is the limiting form (in the limit of a complete set of reference velocities) of the interpolation algorithm of Gazdag and Squazzerro (1984). Another important property is that GPSPI is also the limiting form (in the limit of an infinitely long operator) of (x, ω) explicit finite-difference wavefield extrapolation (Etgen, 1994). Furthermore, the generalized screen propagators (GSP1 and GSP2) of Le Rousseau and de Hoop (2001) are both approximate realizations of GPSPI. So, in a broad sense, the comparison to GPSPI is a comparison to the best extrapolation techniques that are in current practice. The NSPS algorithm is the spatial transpose of GPSPI in the (x, ω) domain. The Weyl algorithm is intermediate to NSPS and GPSPI and is patterned after a form proposed by Weyl (1931) for a self-adjoint pseudodifferential operator in Quantum mechanics.

These three approximate extrapolators are distinguished by how they handle the velocity field in taking a single depth step. Let \hat{x} denote the set of lateral coordinate positions of each grid point at the starting depth level and let x denote the set of lateral coordinate positions at the extrapolated depth level. By \hat{x}_k and x_k we refer to particular points in the input or output grids. GPSPI computes the extrapolated wavefield for a specific point x_k by propagating the data on straight raypaths from each point in \hat{x} to x_k using constant velocity along each ray given by the velocity at x_k (i.e. at the end of each ray). In contrast, NSPS images the same point in x with the same straight raypaths but assumes a constant velocity along the k^{th} raypath given by the velocity at \hat{x}_k (i.e. at the beginning of each ray). Finally, the Weyl operator also uses the same straight raypaths but uses the average of the velocities at the beginning and ends of each ray.

Figures 4, 5, and 6 show the results of single 200 m upward steps² with NSPS, GPSPI, and Weyl respectively. Though grossly wrong in comparison with the exact answer (Figure 3) these results are exactly as expected from the known approximations in these two algorithms. NSPS extrapolates the wavefield using locally constant velocity as a function of the *input* coordinate. This means that each impulse in the input wavefield is

² A 200 m extrapolation step is about 20 times larger than standard practice but is used here to exaggerate the effects for easier comparison.

pushed out (propagated upward) with the velocity at the x-location of the impulse. Since the single impulse here is in the low-velocity medium, the result is a single low-velocity hyperbola. In contrast, GPSPI extrapolates using the lateral velocity variation at the output coordinate. The result is that the single input impulse is *drawn upward* at the velocity appropriate for each output coordinate. The result is a discontinuous response with the discontinuity exactly at the velocity interface. Finally, the Weyl extrapolator produces a result that is intermediate to those of NSPS and GPSPI.

While all three of these results are clearly wrong, it is interesting to observe that if the approximate extrapolators are applied in a recursive series of smaller steps, the result is much more like the exact answer. This is shown in Figures 7, 8, and 9 where each of the algorithms took ten, 20 m upward steps. Comparison with Figure 3 shows that each algorithm has formed a reasonable approximation to the exact result.

Figures 10, 11, and 12 show in more detail how these approximate algorithms converge upon the correct answer as the step size becomes smaller. For each algorithm, four panels are shown giving the results of 1, 2, 5, and 10 steps over a total distance of 200 meters. (The 1 step and 10 step results are the same as already shown in previous figures). These figures are shown with some amplitude clipping in order to make the details more obvious. Figure 13 shows the results from the exact extrapolator for each of these four instances. The exact extrapolator produces an identical result regardless of the number of steps taken.

Figure 14 shows an input wavefield containing 8 impulses whose extrapolations through the step velocity model (Figure 1) are shown in the next four figures. Figure 15 shows an exact extrapolation 200 m upwards. Of particular note is the refraction of the diffraction tails as they cross the velocity discontinuity. In comparison, the NSPS result in Figure 16 has the diffraction tails crossing the velocity discontinuity without any refraction. In Figure 17, the GPSPI result has an extreme discontinuity in the wavefield at the velocity discontinuity. Though the GPSPI result appears less physical than NSPS, the results shown previously suggest that both converge to the right answer in a similar number of steps. The Weyl extrapolation in Figure 18 has again produced a result that is intermediate to NSPS and GPSPI.

Figure 19 shows a more complex velocity model created by superimposing a random (normally distributed) fluctuation with standard deviation of 500 m/s on top of the step model of Figure 1. This *noisy step* model was then lowpass-filtered to pass only wavenumbers up to 10% Nyquist to create the *filtered step* model. Figure 20 is a 200 m upward exact extrapolation through the filtered step model while Figure 21 is a similar result but the noisy step model was used.

As a final test of the approximate extrapolators, we illustrate their abilities to focus, through downward extrapolation, the exact upward extrapolations created with the three velocity models: velocity step (Figure 1) and the noisy step and filtered step (Figure 19). In each case, we tested each approximate extrapolator by stepping down 200 m in either 1, 2, 5, or 10 steps.

Figures 22, 23, and 24 show the results using the NSPS, GPSPI, and Weyl extrapolators for the step velocity model with the wavefield of Figure 16 as input. We

have compressed the output to show four extrapolations in a single figure. Somewhat surprisingly, it appears that NSPS has done the best job of imaging the point just to the right of the velocity discontinuity. All three extrapolators have done a similar job elsewhere.

Figures 25, 26, and 27 are the results using the three extrapolators for the filtered step model with the wavefield of Figure 20 as input. This time, after 1 step, only the Weyl extrapolator has produced a result on which all eight focal points can be distinguished. Even after 2 steps, Weyl is still clearly better. After 5 and again after 10 steps, it appears that NSPS has become as clear as Weyl while GPSPI is slightly inferior.

Figures 28, 29, and 30 perform this same test using the noisy step model (Figure 19) and the wavefield of Figure 21 as input. This is a very extreme test and all three extrapolators failed to produce an image on which all eight focal points could be identified. The extrapolators had more trouble on the low velocity side (left) than on the high velocity side. Examining the three results after 10 steps, it appears that GPSPI is again slightly inferior to the other two extrapolators.

Figure 31 shows that the exact extrapolator inverts itself exactly using any number of steps. We use the word “exactly” here with some reservation because we did not invert the evanescent velocity field but simply extrapolated downward with the evanescent field still being attenuated. The result is independent of the number of recursive steps taken over the 200 m interval (as it should be). In the case of the noisy step model, there does appear to be some reduction in amplitude of the fifth focal point.

In Figures 32, 33, and 34 we simulate running the extrapolators with an erroneous velocity model. In Figure 32 are results from all four extrapolators using the data from the noisy step model (Figure 21) and the filtered step velocity model. Thus the velocity model is much smoother than the correct model, a circumstance that is probably common with real data. It appears that the exact extrapolator has produced a better image but only marginally so. In Figure 33, the noisy step data has been inverted with the step velocity model, an even more smoothed model except for the discontinuity. Here we see almost identical performance from the four extrapolators. (The exact extrapolator gets this result in one step while the approximate ones require 10 steps.) A very similar story emerges in Figure 34 where we have used the data from the filtered step and the step velocity model.

CONCLUSIONS

The 2D, discrete wavefield extrapolation problem can be solved exactly for arbitrary lateral velocity variations. The solution is developed via an eigenvalue decomposition in the Fourier domain. The matrix that is decomposed is the difference between a diagonal matrix containing the squared horizontal wavenumbers and a Toeplitz matrix, scaled by frequency squared, containing the Fourier transform of the square on the inverse velocity. This solution gives an explicit decomposition of a wavefield into independent upward and downward travelling parts.

We also analyze the continuous problem via functional analytic methods and, though we fail to reach a general solution, we demonstrate the independence of upward and downward-travelling waves. In the specific case of the step velocity function, we

calculate the eigenfunctions and exhibit a formula that determines the eigenvalues, though the latter must be solved numerically.

Numerical testing shows that the exact extrapolator produces physically understandable result. When compared with three different approximate extrapolators based on Fourier integral operators, the approximate operators can be grossly wrong if a large extrapolation step is taken in the presence of strong velocity gradients. However, if the approximate operators are used in a recursion taking many small steps, they appear to approach the correct result. In a simulation of inversion with an erroneous velocity model, the three approximate extrapolators produce a very similar result to the exact extrapolator. This indicates that a very precise velocity model is required to take advantage of the exact extrapolator.

ACKNOWLEDGEMENTS

Funding for this work came from CREWES, POTSI, NSERC, and MITACS and we thank all of these organizations.

REFERENCES

- Berkhout, A.J., 1981, Wave field extrapolation techniques in seismic migration, a tutorial: *Geophysics*, **46**, 1638-1656.
- Berkhout, A.J., 1985, Seismic Migration: Imaging of acoustic energy by wave field extrapolation: in *Developments in Solid Earth Geophysics*, Vol. 14A, Elsevier.
- Bevc, D. 1997, Imaging complex structures with semirecursive Kirchhoff migration: *Geophysics*, **62**, 577-588.
- Claerbout, J, 1976, *Fundamentals of Geophysical Data Processing*: McGraw-Hill.
- Ferguson, R.J. and Margrave, G.F., 2002, Prestack depth migration by symmetric nonstationary phase shift: *Geophysics*, **67**, 594-603.
- Fishman, L. and McCoy, J.J., 1985, A new class of propagation models based on a factorization of the Helmholtz equation: *Geophys. J. Astr. Soc.*, **80**, 439-461.
- Gazdag, J., 1978, Wave equation migration with the phase-shift method: *Geophysics, Soc. of Expl. Geophys.*, **43**, 1342-1351.
- Gazdag, J. and Sguazero, P., 1984, Migration of seismic data by phase shift plus interpolation: *Geophysics*, **49**, 124 - 131.
- Grimbergen, J.L.T., Dessing, F.J., and Wapenaar, C.P.A., 1998, Modal expansion of one-way operators in laterally varying media: *Geophysics*, **63**, 995-1005.
- Le Rousseau, J.H. and de Hoop, M.V., 2001, Modeling and imaging with the scalar generalized-screen algorithms in isotropic media: *Geophysics, Soc. of Expl. Geophys.*, **66**, 1551-1568.
- Margrave, G.F. and Ferguson, R.J., 1998, Explicit Fourier wavefield extrapolators: *CREWES Research Report*, Vol. **10**.
- Margrave, G.F. and Ferguson, R.J., 1999, Wavefield extrapolation by nonstationary phase shift: *Geophysics*, **64**, 1067-1078.
- Margrave, G.F. and Daley, P.F., 2001, Recursive Kirchhoff wavefield extrapolation: *CREWES Research Report*, Vol. **13**.
- Margrave, G.F. and Geiger, H.D., 2002, Wavefield resampling during Kirchhoff extrapolation: *CREWES Research Report*, Vol. **14**.
- Stoffa, P.L., Fokkema, J.T., de Luna Freire, R.M., and Kessinger, W.P., 1990, Split-step Fourier migration: *Geophysics*, **55**, 410-421.
- Strang, G., 1986, *Introduction to Applied Mathematics*: Wellesley-Cambridge Press, ISBN 0-9614088-0-4.
- Weyl, H., 1931, *The Theory of Groups and Quantum Mechanics*: Dover edition (pub 1950).
- Wu, R.S., 1992, Scattered field calculation in heterogeneous media using a phase-screen propagator: 62nd Annual Internat. Mtg., Soc. Expl. Geophys., Expanded Abstracts, 1289 - 1292.

- Wu, R.S., 1994, Synthetic seismograms in heterogeneous media by one-return approximation: *Pure and Appl. Geophysics*, **148**, 155-173.
- Yao, Z. and Margrave, G. F., 1999, Wavefield extrapolation in laterally inhomogeneous media by generalized eigenfunction transform method: *CREWES Research Report*, Vol. **11**
- Yao, Z. and Margrave, G.F., 2000, Wavefield extrapolation in laterally inhomogeneous media by generalized eigenfunction transform method: *GeoCanada 2000 Expanded Abstracts*.

FIGURES

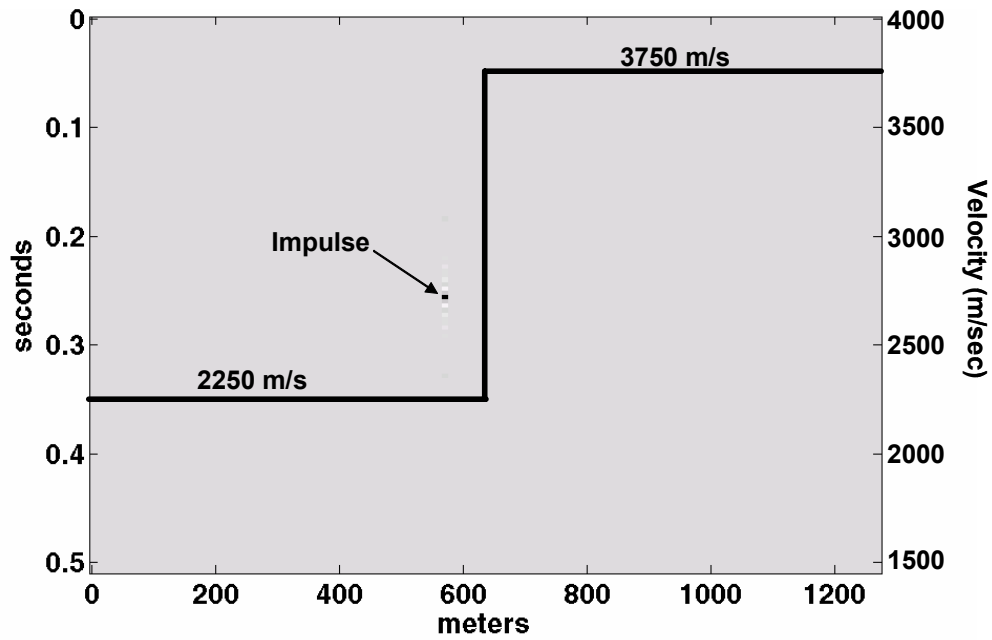


FIG. 1: The input wavefield and the velocity model for Figures 2-18

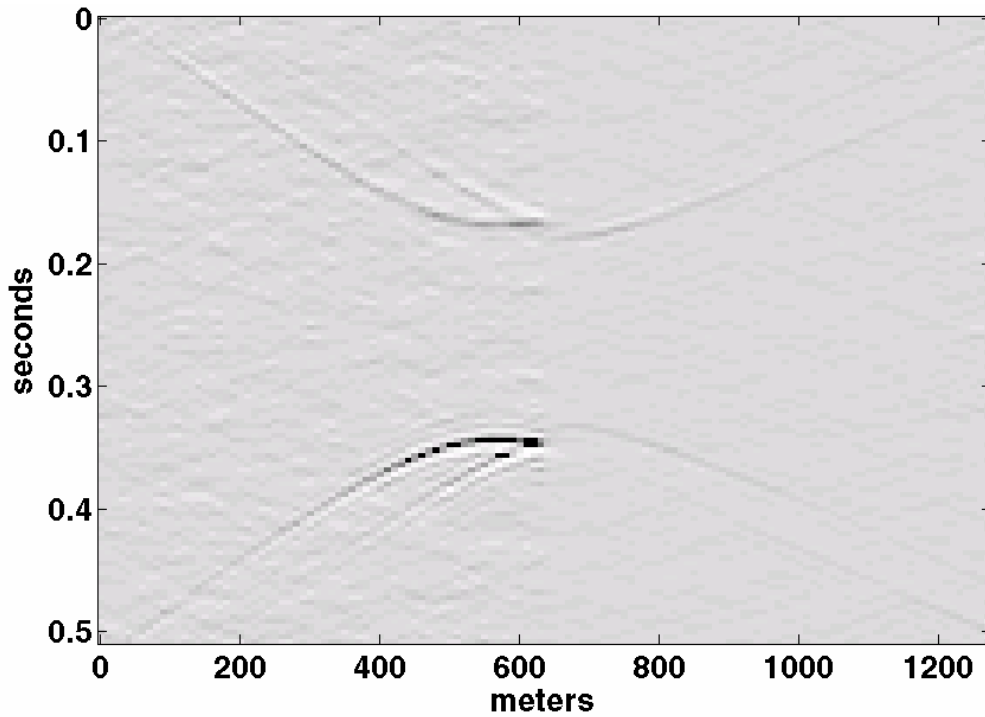


FIG. 2: After extrapolation of the wavefield of Figure 1 upward 200 m using the step velocity field also shown in Figure 1.

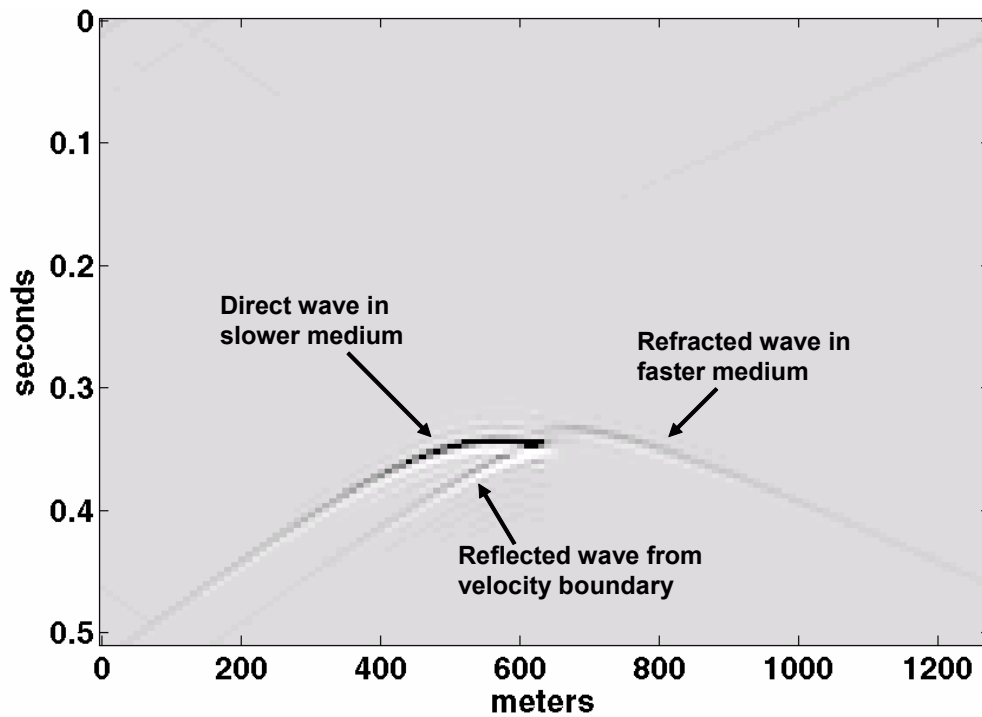


FIG. 3: Similar to Figure 2 except the velocity field was given an imaginary component of 1% of the real component.

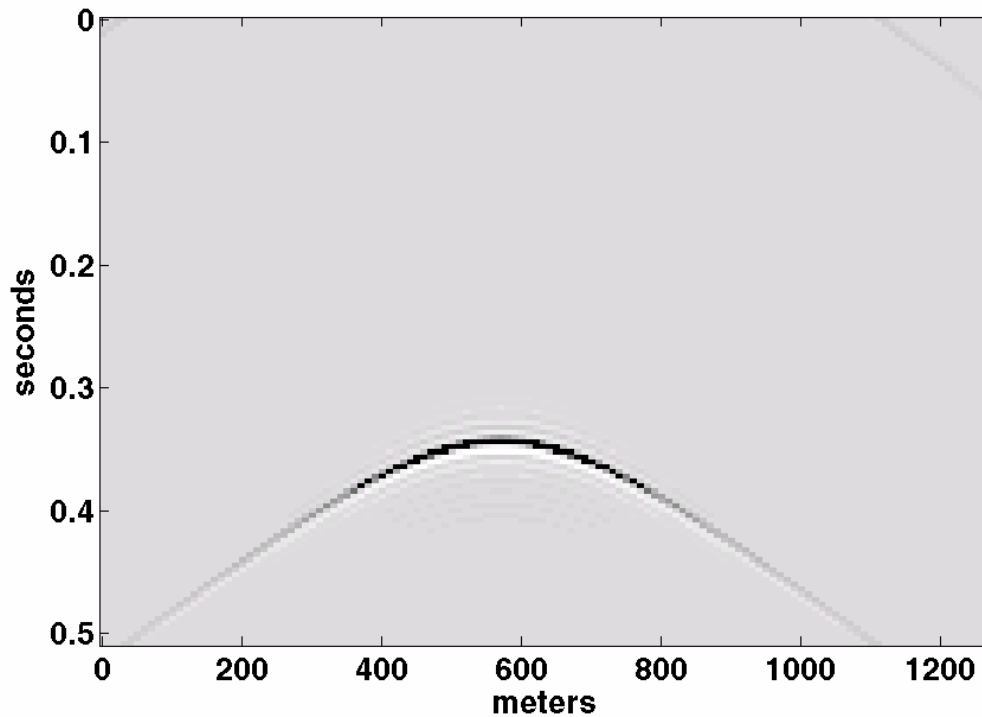


FIG. 4: A result comparable to that of Figure 3 except that the approximate NSPS extrapolator of Margrave and Ferguson (1999) was used.

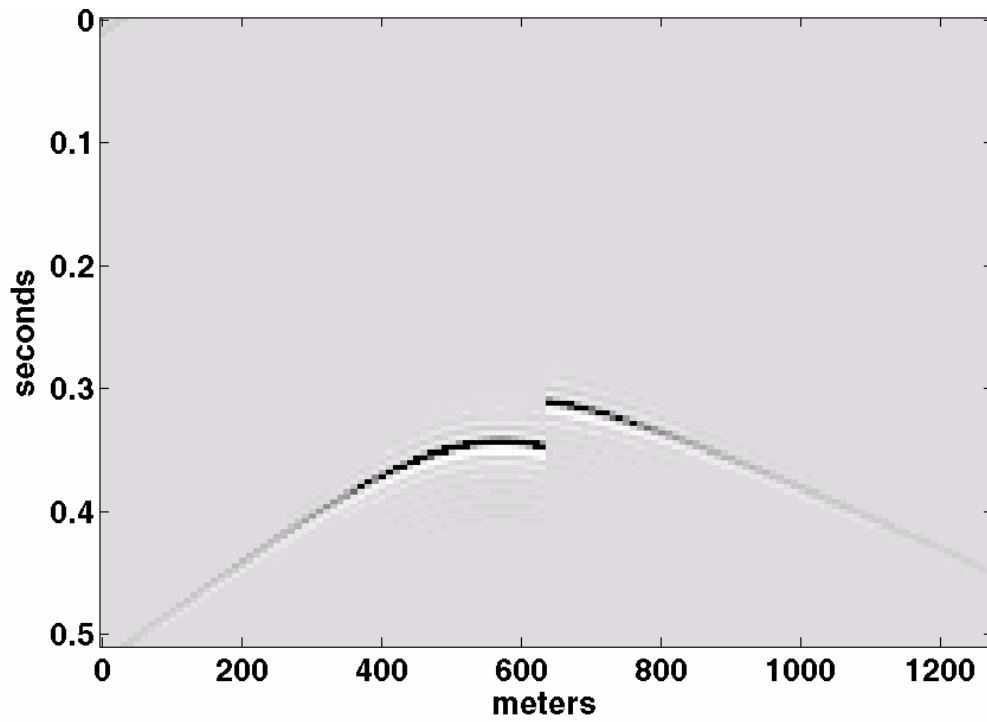


FIG. 5: A result comparable to that of Figure 4 except that the approximate PSPI extrapolator of Margrave and Ferguson (1999) was used.

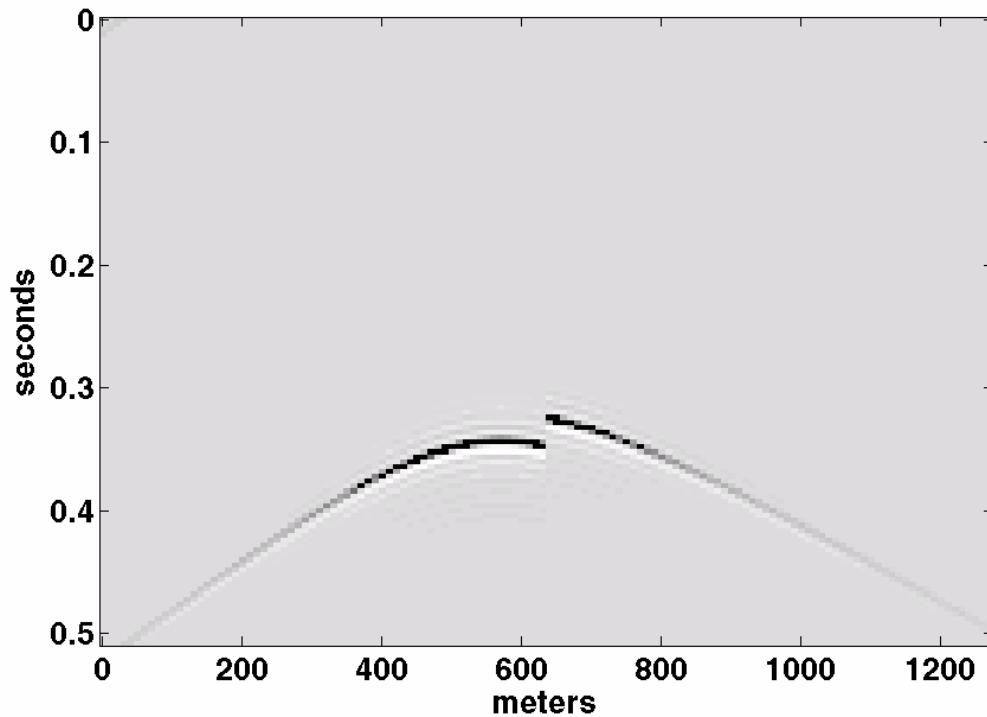


FIG. 6: A result comparable to that of Figure 4 except that the approximate Weyl extrapolator was used.

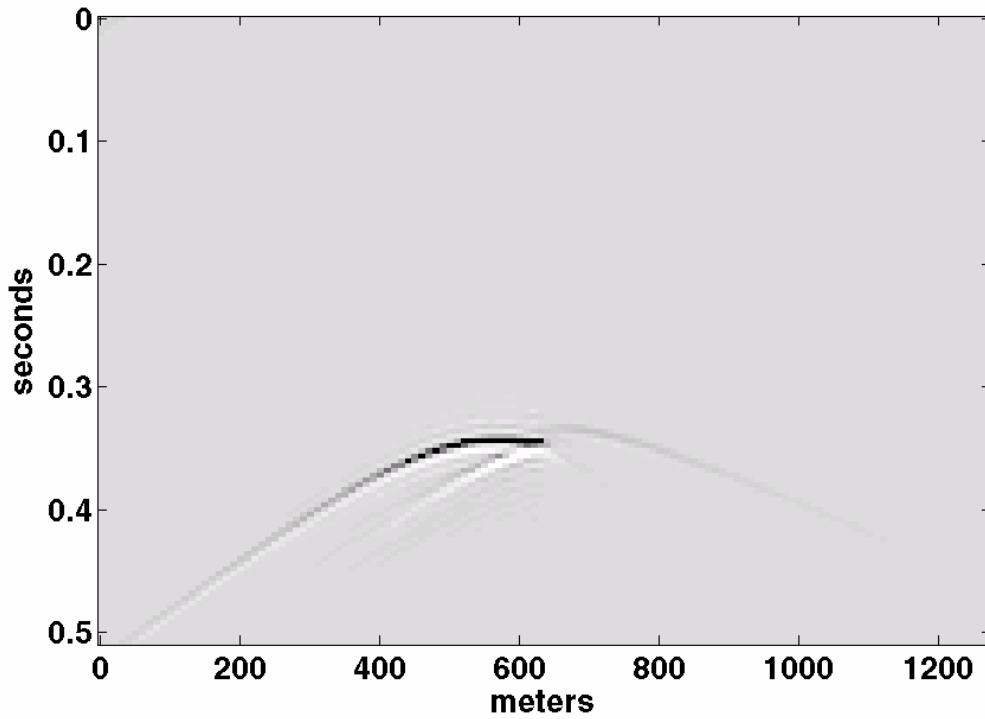


FIG. 7: The result from 10 steps of 20 metres each in the upward direction using the NSPS algorithm. Compare with Figures 3 and 4.

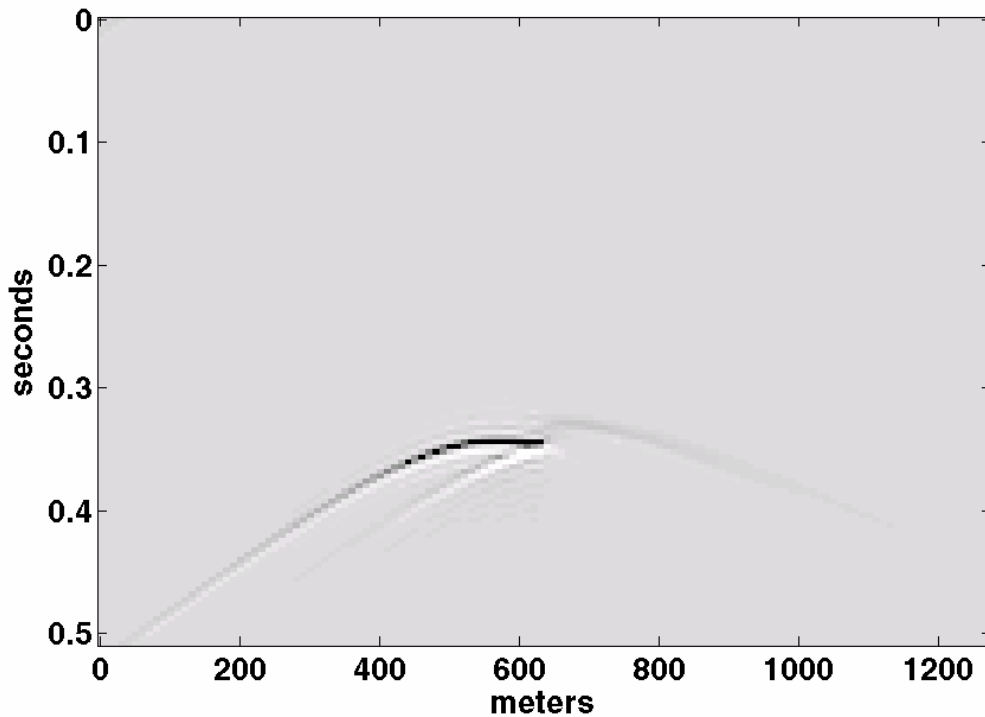


FIG. 8: The result from 10 steps of 20 metres each in the upward direction using the PSP algorithm. Compare with Figures 3 and 5.

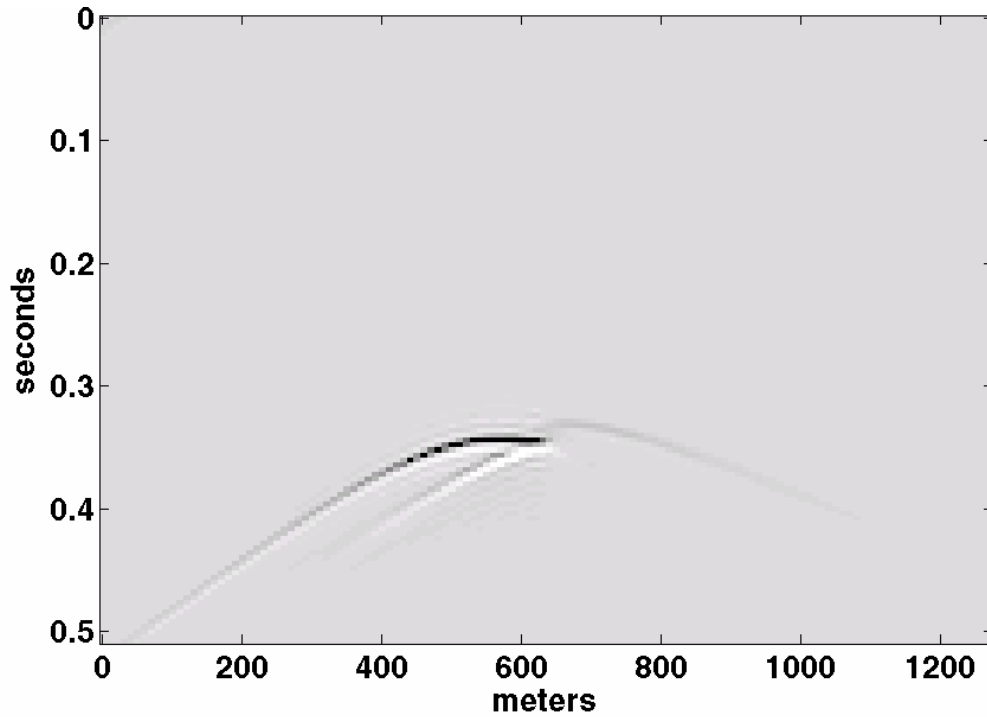


FIG. 9: The result from 10 steps of 20 metres each in the upward direction using the Weyl algorithm. Compare with Figures 3 and 6.

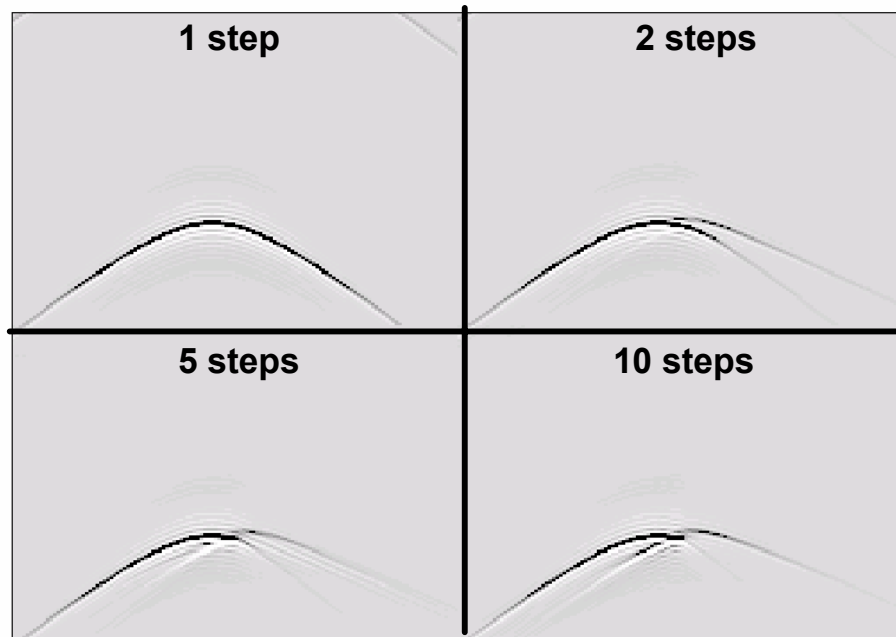


FIG. 10: Variation with number of steps of the NSPS solution for the model of Figure 1. Each panel shows the result of a 200 m upward extrapolation with the indicated number of steps. In each case, the actual step size was $200\text{m}/(\text{number of steps})$. These results are clipped to show detail.

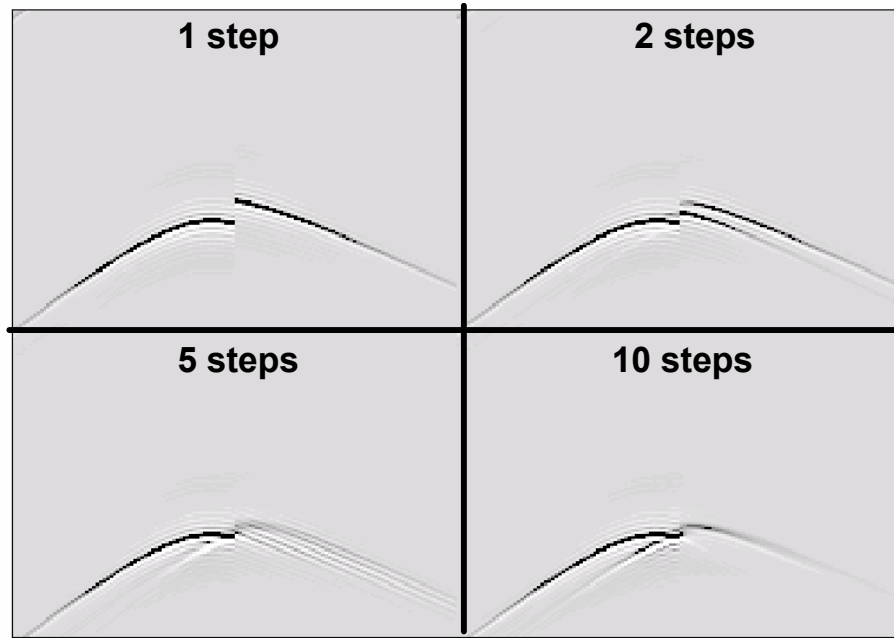


FIG. 11: Similar to Figure 10 except that the PSPI algorithm was used.

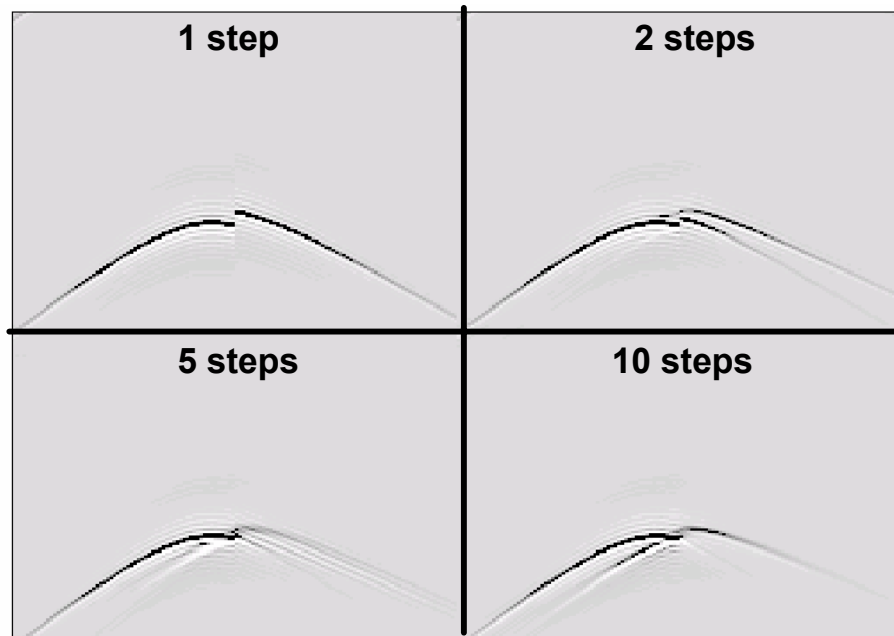


FIG. 12: Similar to 10 except that the Weyl algorithm was used.

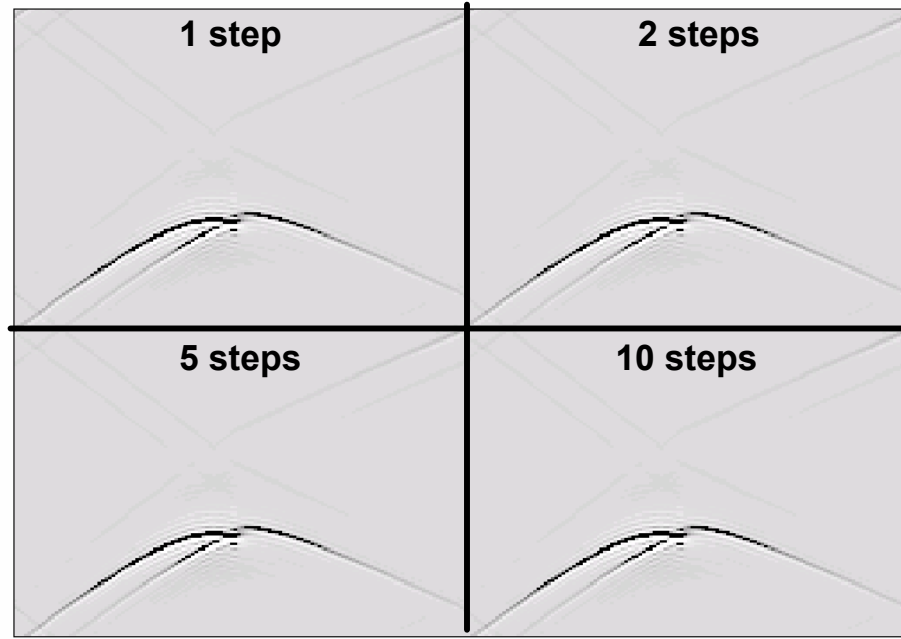


FIG. 13: Similar to 10 except that the exact algorithm was used. Unlike the approximate extrapolators, the exact extrapolator gets the same result independent of the number of steps.

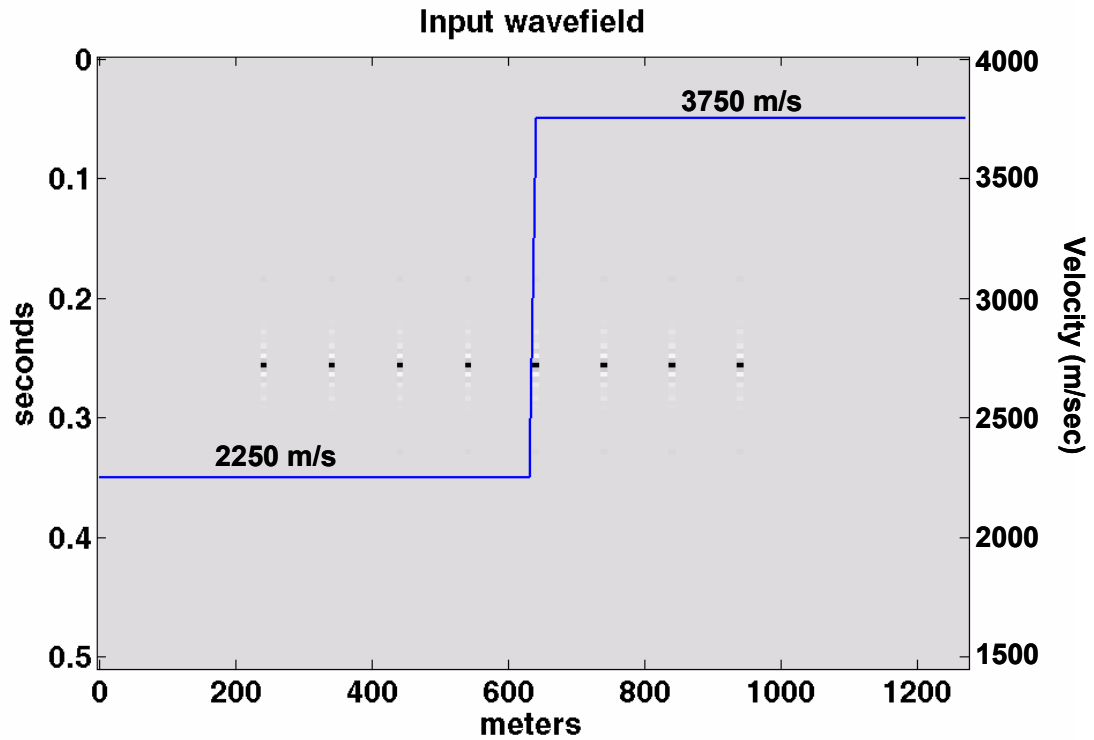


FIG. 14: An input wavefield containing 8 bandlimited impulses.

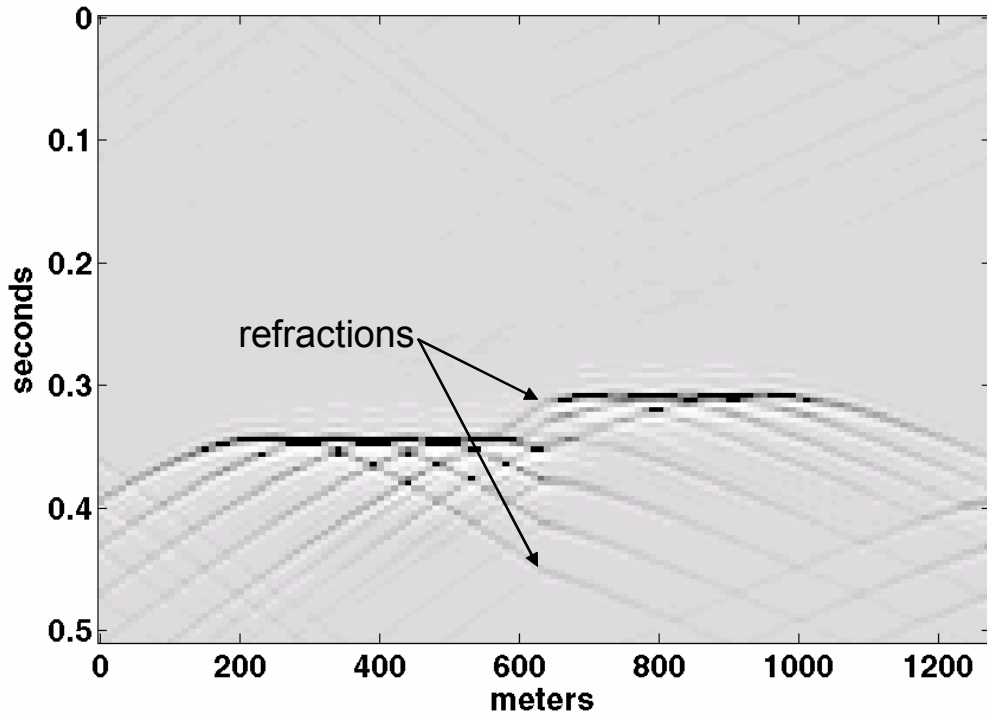


FIG. 15: An exact extrapolation of the wavefield of Figure 14 through the step velocity model of Figure 1. Note the refractions of the diffraction tails as they cross the velocity discontinuity. Two are noted explicitly.

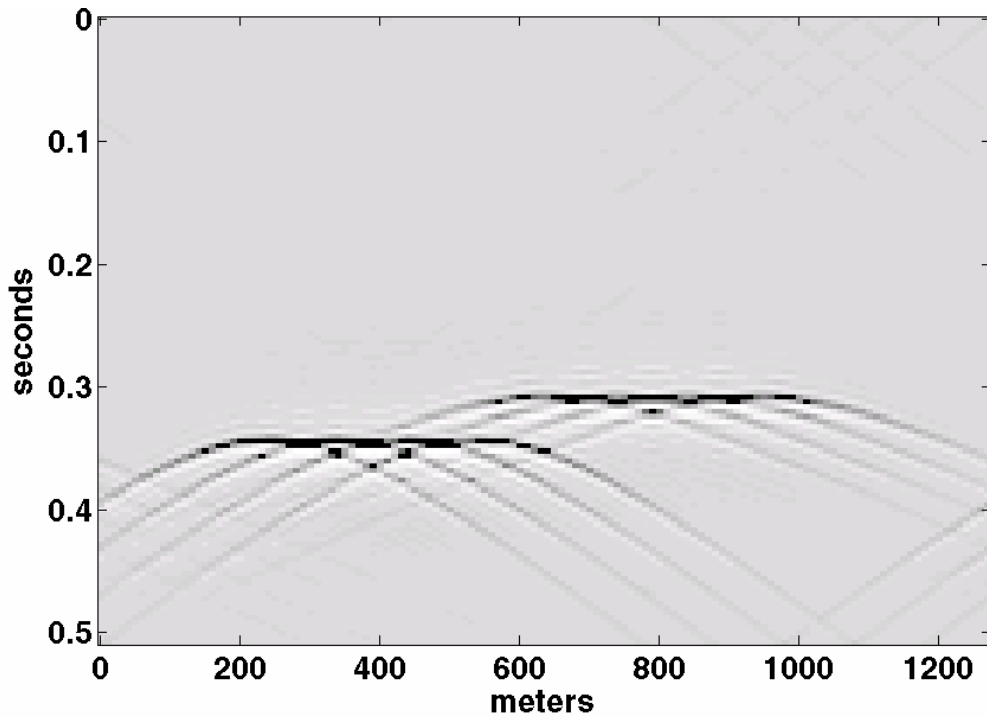


FIG. 16: An NSPS extrapolation of the wavefield of Figure 14 through the step velocity model of Figure 1.

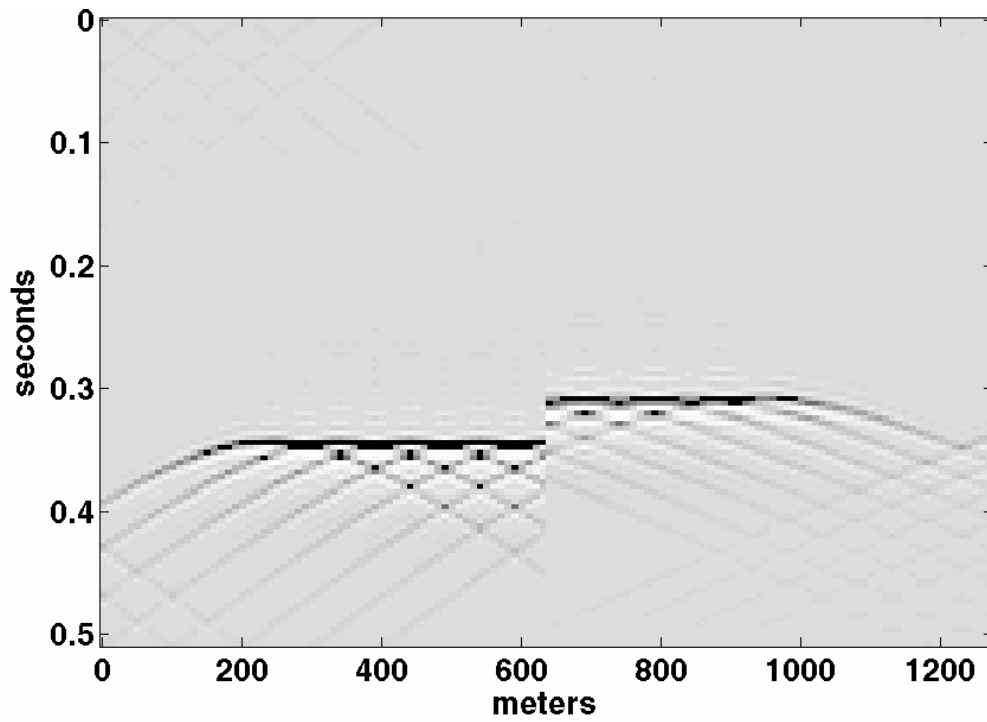


FIG. 17: A PSPI extrapolation of the wavefield of Figure 14 through the step velocity model of Figure 1.

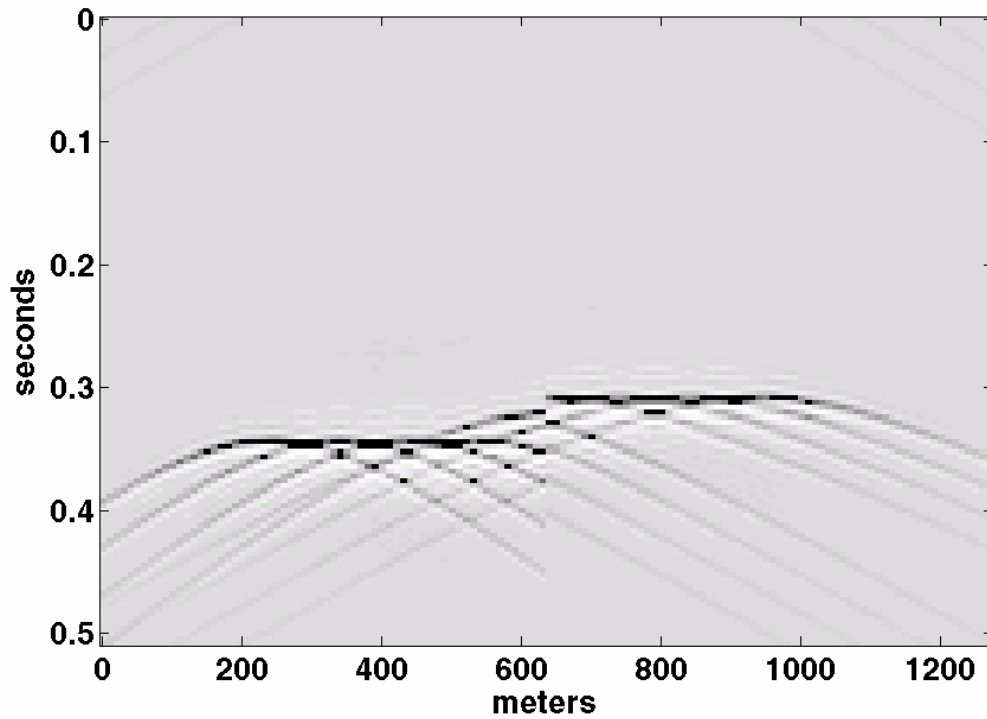


FIG. 18: A Weyl extrapolation of the wavefield of Figure 14 through the step velocity model of Figure 1.

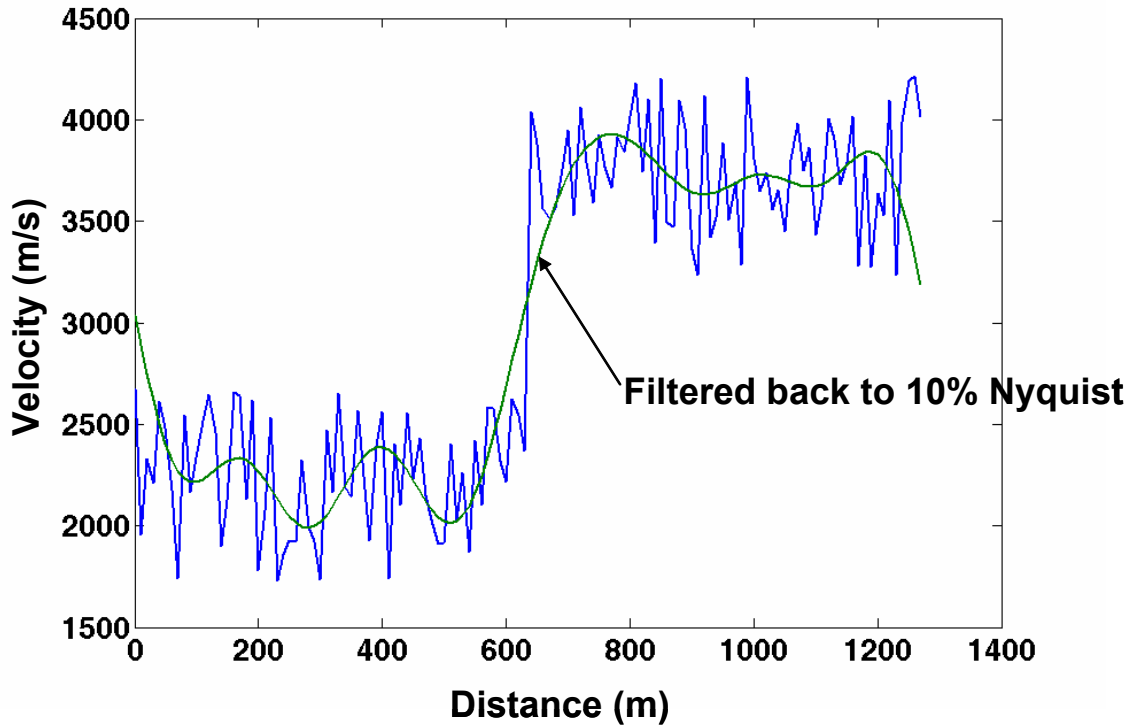


FIG. 19: The step velocity model of Figure 1 has been altered with a random fluctuation 500 m/s (standard deviation) and then lowpass-filtered to 10% of Nyquist. These will be called the 'noisy step' and the 'filtered step' models.

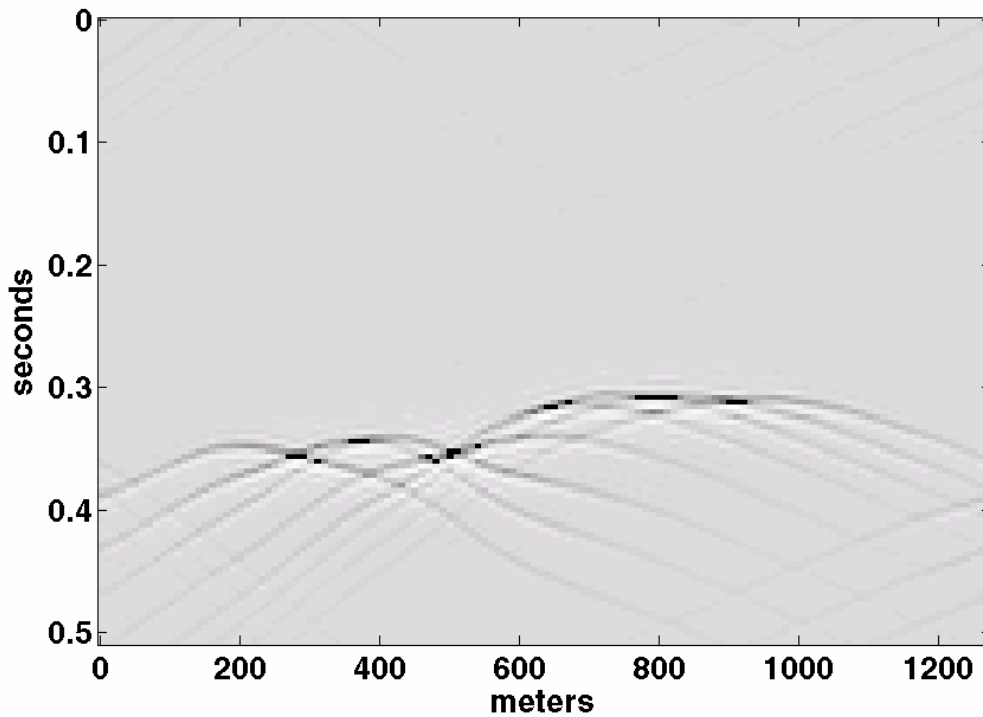


FIG. 20: The exact extrapolation of the wavefield of Figure 14 after a 200 m upward step through the filtered step velocity model of Figure 19.

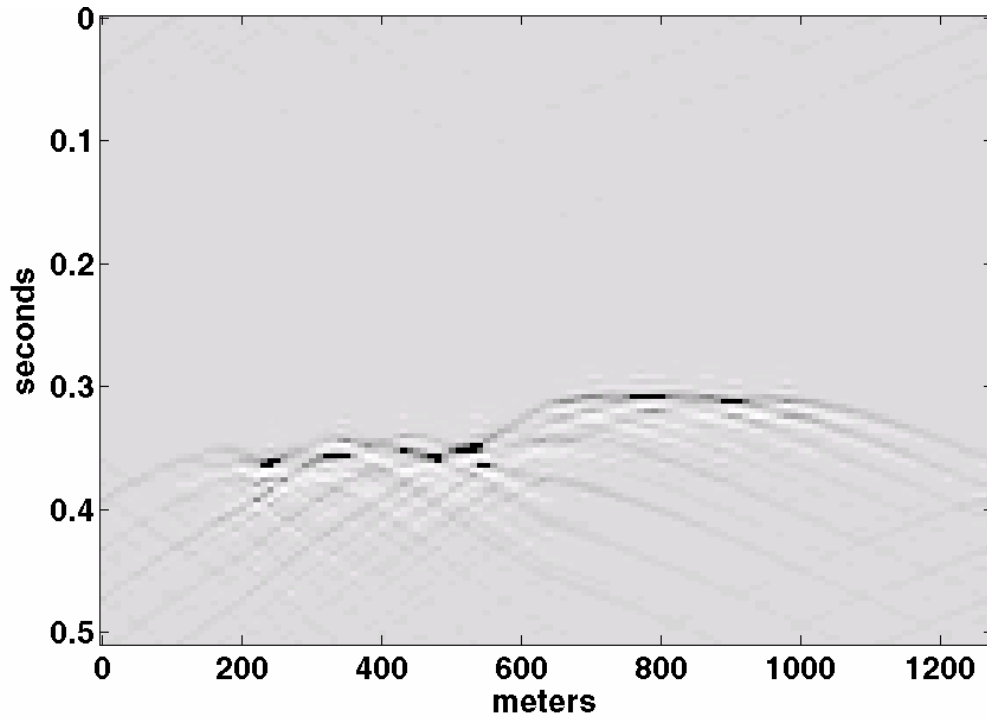


FIG. 21: The exact extrapolation of the wavefield of Figure 14 after a 200 m upward step through the noisy step velocity model of Figure 19. Compare with Figure 20.

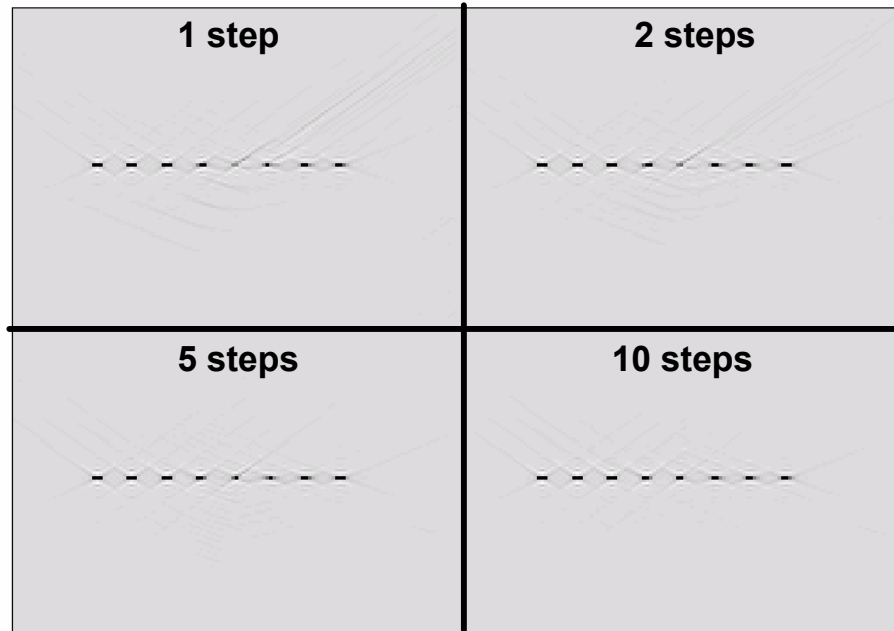


Fig 22: Four different 200 m downward extrapolations with the NSPS extrapolator using the indicated number of steps. The input was the wavefield of Figure 16 and the velocity was the velocity step of Figure 1.

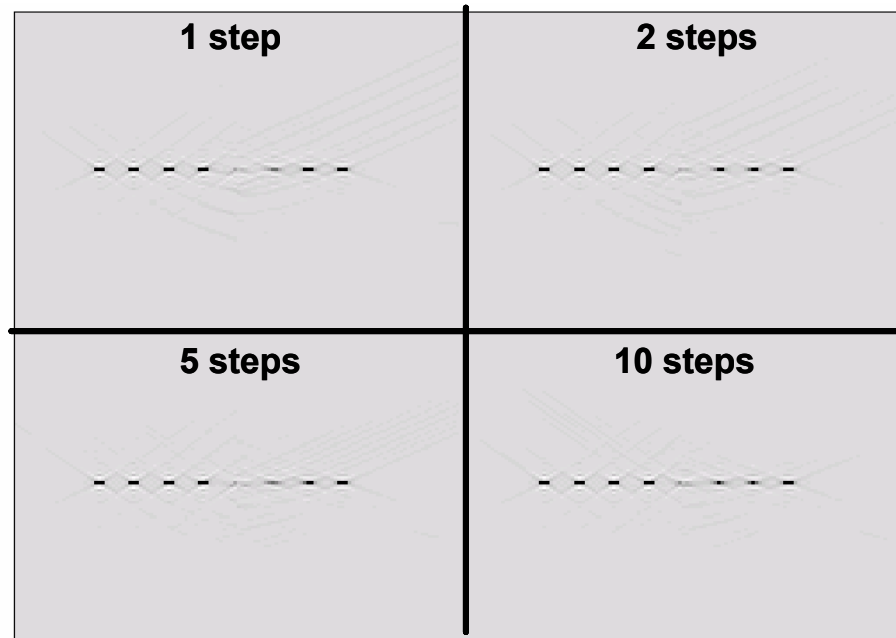


Fig 23: Four different 200 m downward extrapolations with the GPSPI extrapolator using the indicated number of steps. The input was the wavefield of Figure 16 and the velocity was the velocity step of Figure 1.

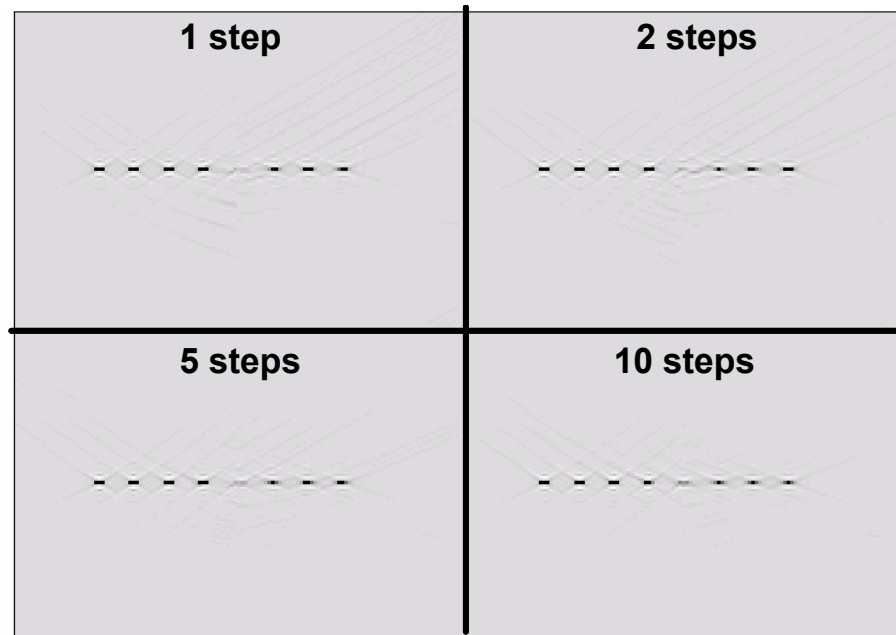


Fig 24: Four different 200 m downward extrapolations with the Weyl extrapolator using the indicated number of steps. The input was the wavefield of Figure 16 and the velocity was the velocity step of Figure 1.

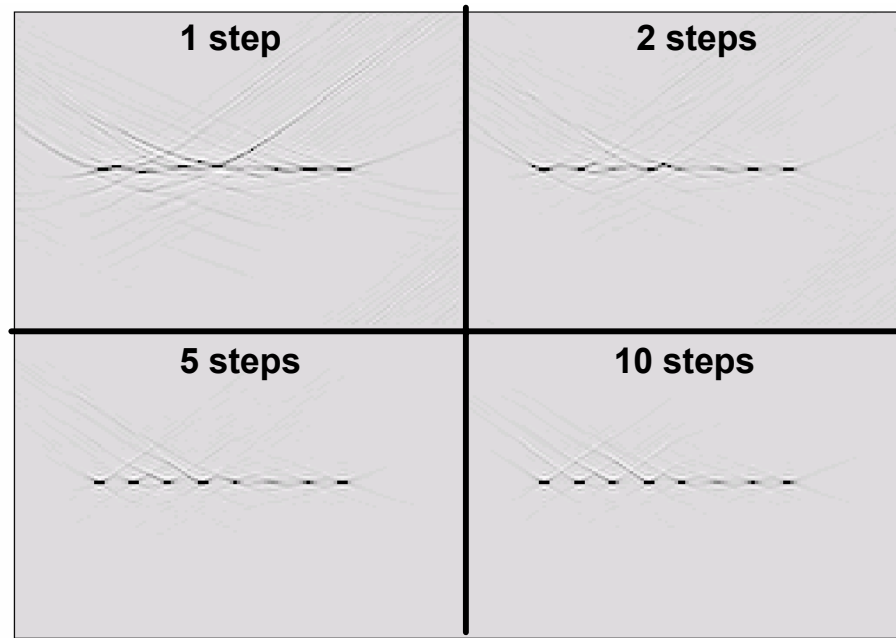


Fig 25: Four different 200 m downward extrapolations with the NSPS extrapolator using the indicated number of steps. The input was the wavefield of Figure 20 and the velocity was the filtered velocity step of Figure 19.

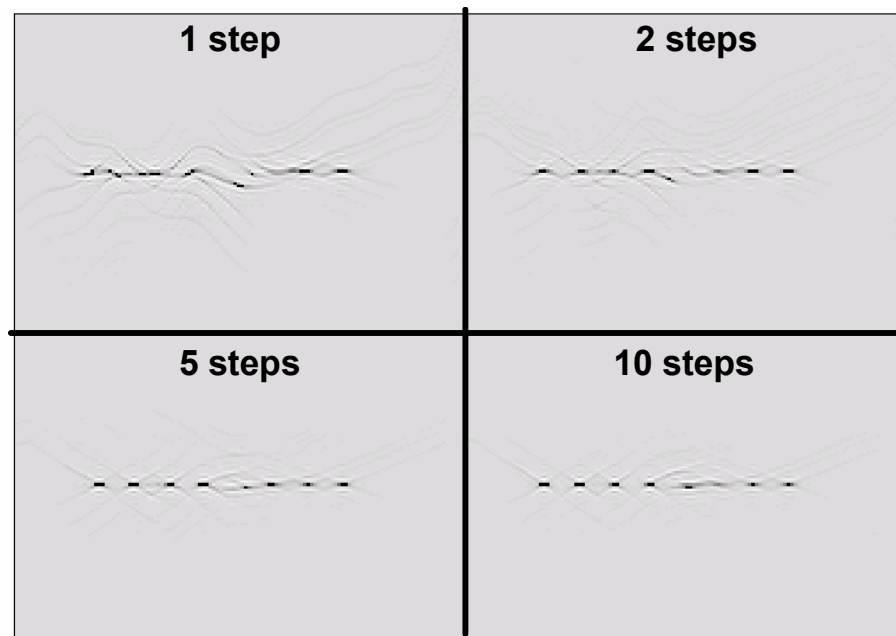


Fig 26: Four different 200 m downward extrapolations with the GPSP extrapolator using the indicated number of steps. The input was the wavefield of Figure 20 and the velocity was the filtered velocity step of Figure 19.

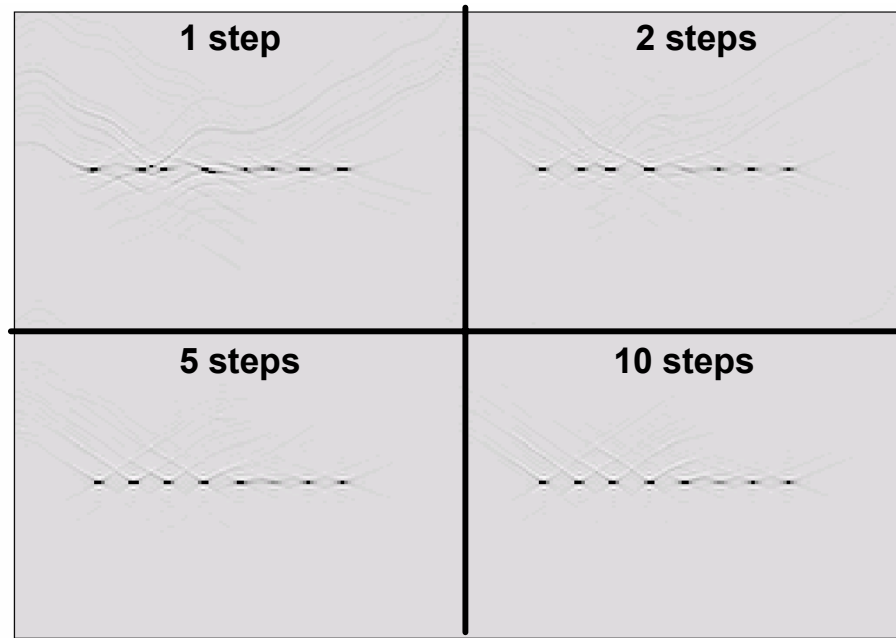


Fig 27: Four different 200 m downward extrapolations with the Weyl extrapolator using the indicated number of steps. The input was the wavefield of Figure 20 and the velocity was the filtered velocity step of Figure 19.

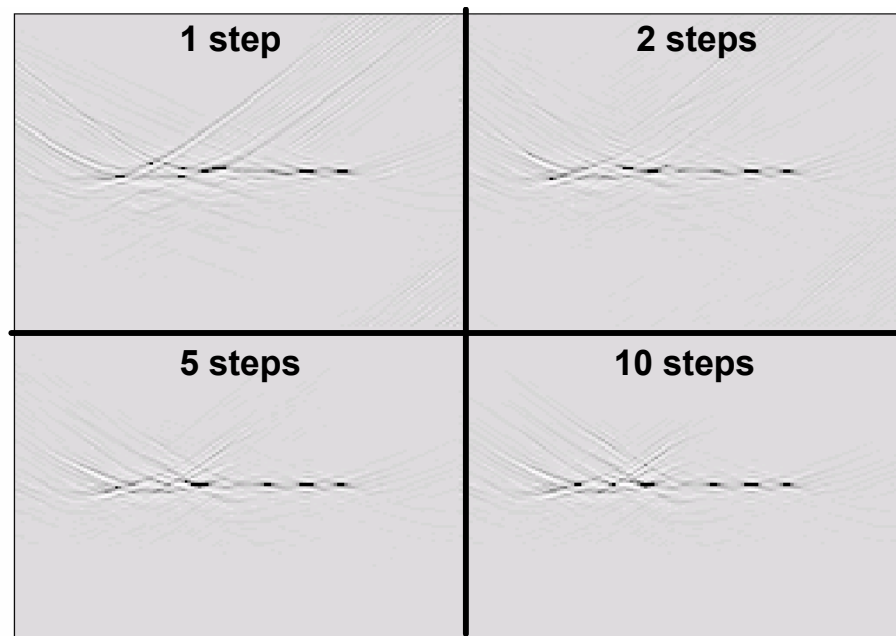


Fig 28: Four different 200 m downward extrapolations with the NSPS extrapolator using the indicated number of steps. The input was the wavefield of Figure 21 and the velocity was the noisy velocity step of Figure 19.

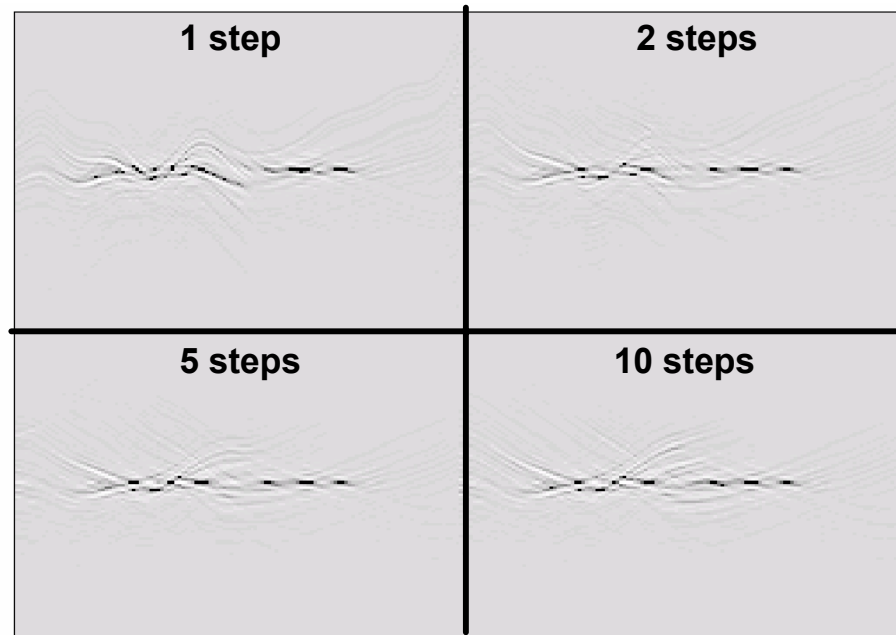


Fig 29: Four different 200 m downward extrapolations with the GPSPI extrapolator using the indicated number of steps. The input was the wavefield of Figure 21 and the velocity was the noisy velocity step of Figure 19.

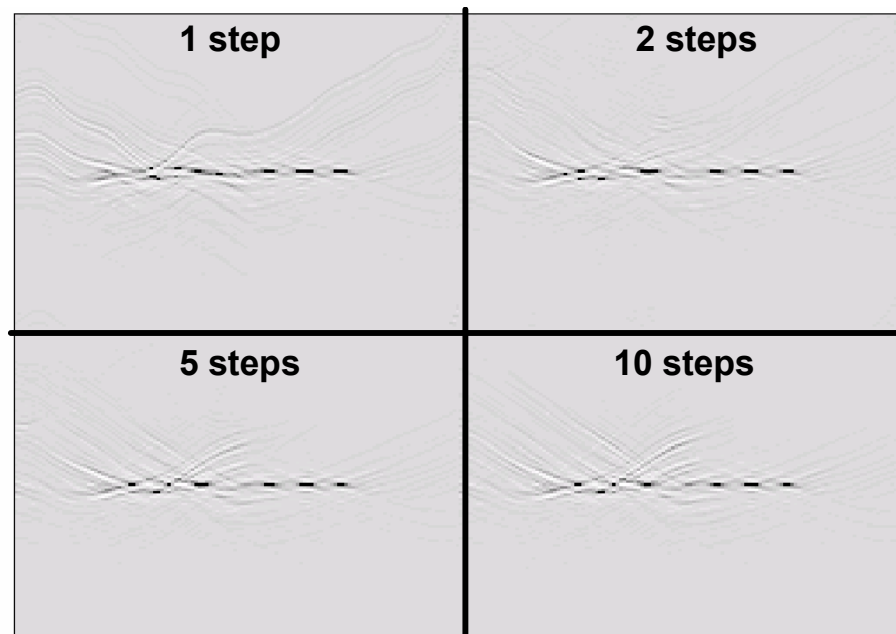


Fig 30: Four different 200 m downward extrapolations with the Weyl extrapolator using the indicated number of steps. The input was the wavefield of Figure 21 and the velocity was the noisy velocity step of Figure 19.

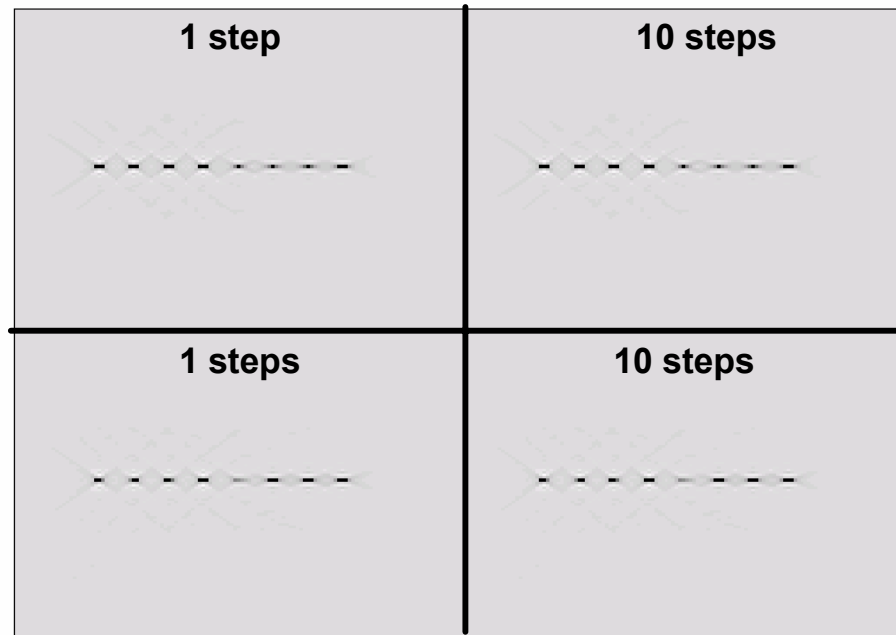


Fig 31: Top: The result of an exact downward extrapolation of the wavefield of Figure 20 using the filtered step velocity model. Bottom: The result of the exact downward extrapolation of the wavefield of Figure 21 using the noisy step velocity model.

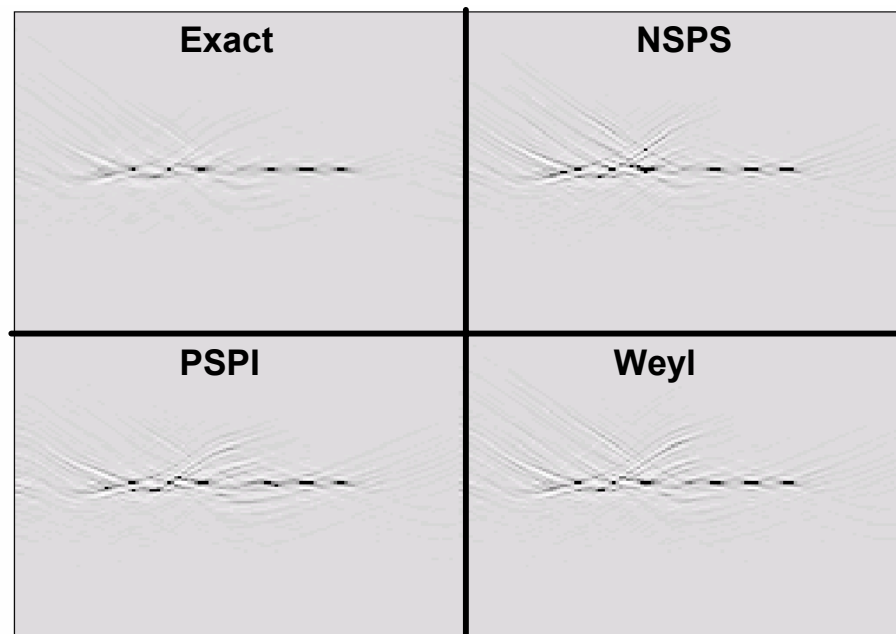


FIG. 32: The results of four different 200 m downward extrapolations in 10 steps of the wavefield in Figure 21 using the filtered step velocity model of Figure 19.

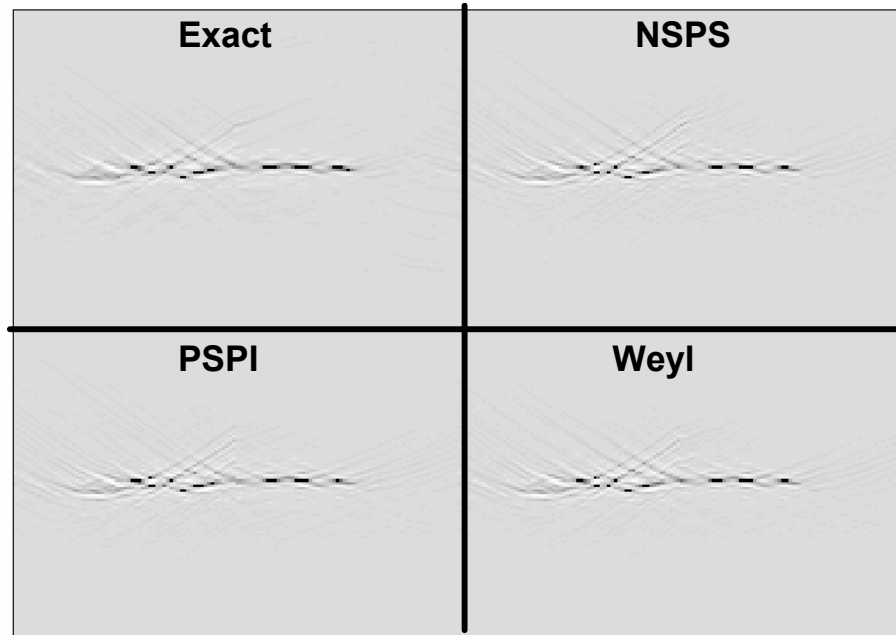


FIG. 33: The results of four different 200 m downward extrapolations in 10 steps of the wavefield in Figure 21 using the step velocity model of Figure 1.

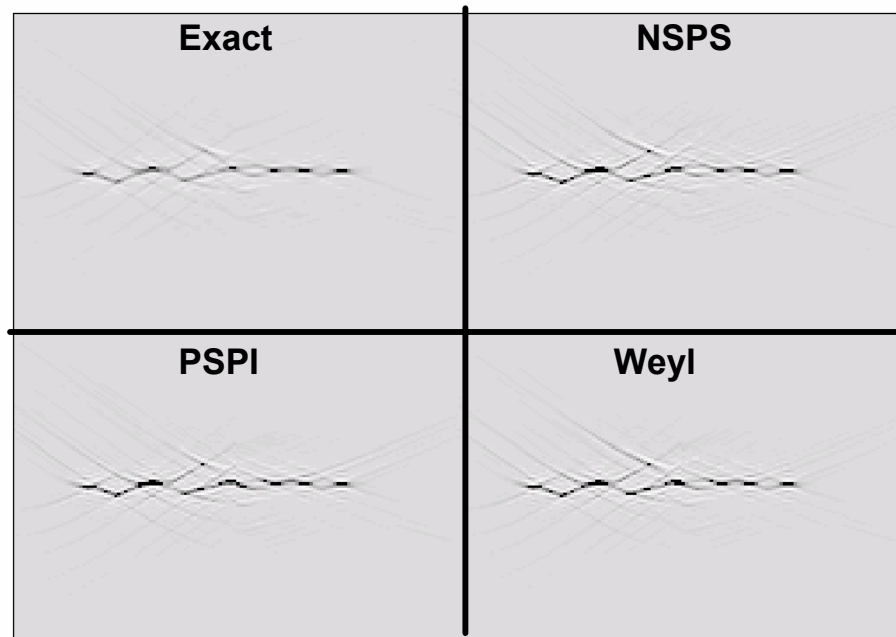


FIG. 34: The results of four different 200 m downward extrapolations in 10 steps of the wavefield in Figure 20 using the step velocity model of Figure 1.